

# Measurement of $B_d^0 - \overline{B}_d^0$ oscillations

DELPHI Collaboration

## Abstract

$B_d^0$  meson oscillations are measured in hadronic  $Z^0$  decays using the charge of a lepton or the mean charge of an event hemisphere to sign the presence of a  $b$  or a  $\bar{b}$  quark when it is produced, and using the charge of a lepton emitted at large  $p_t$  or of a  $D^{*\pm}$  to sign the presence of a  $B$  or a  $\bar{B}$  meson when it decays. With 3.2 million hadronic  $Z^0$  decays registered by DELPHI between 1991 and 1994, the mass difference  $\Delta m_d$  between the two physical  $B_d^0$  states is measured in four channels:

$$\begin{aligned} \Delta m_d &= 0.523 \pm 0.072 \pm 0.043 \text{ ps}^{-1} \quad (D^{*\pm} - Q_{hem}) \\ \Delta m_d &= 0.493 \pm 0.042 \pm 0.027 \text{ ps}^{-1} \quad (\ell - Q_{hem}) \\ \Delta m_d &= 0.499 \pm 0.053 \pm 0.015 \text{ ps}^{-1} \quad ((\pi^* - \ell) - Q_{hem}) \\ \Delta m_d &= 0.480 \pm 0.040 \pm 0.051 \text{ ps}^{-1} \quad (\ell - \ell). \end{aligned}$$

Taking into account the statistical overlap between these measurements and the common systematic uncertainties, the combined result is:

$$\Delta m_d = 0.496 \pm 0.034 \text{ ps}^{-1}.$$

(To be submitted to Zeit. f. Physik C)

P. Abreu<sup>21</sup>, W. Adam<sup>49</sup>, T. Adye<sup>36</sup>, P. Adzic<sup>11</sup>, I. Ajinenko<sup>41</sup>, G. D. Alekseev<sup>16</sup>, R. Alemany<sup>48</sup>, P. P. Allport<sup>22</sup>, S. Almeded<sup>24</sup>, U. Amaldi<sup>9</sup>, S. Amato<sup>46</sup>, P. Andersson<sup>43</sup>, A. Andreazza<sup>9</sup>, P. Antilogus<sup>9</sup>, W.-D. Apel<sup>17</sup>, Y. Arnoud<sup>14</sup>, B. Asman<sup>43</sup>, J.-E. Augustin<sup>25</sup>, A. Augustinus<sup>30</sup>, P. Baillon<sup>9</sup>, P. Bambade<sup>19</sup>, F. Barao<sup>21</sup>, M. Barbi<sup>46</sup>, D. Y. Bardin<sup>16</sup>, G. Barker<sup>9</sup>, A. Baroncelli<sup>39</sup>, O. Barring<sup>24</sup>, M. J. Bates<sup>36</sup>, M. Battaglia<sup>15</sup>, M. Baubillier<sup>23</sup>, J. Baudot<sup>38</sup>, K.-H. Becks<sup>51</sup>, M. Begalli<sup>6</sup>, P. Beilliere<sup>8</sup>, Yu. Belokopytov<sup>9,52</sup>, K. Belous<sup>41</sup>, A. C. Benvenuti<sup>5</sup>, C. Berat<sup>14</sup>, M. Berggren<sup>46</sup>, D. Bertini<sup>25</sup>, D. Bertrand<sup>2</sup>, M. Besancon<sup>38</sup>, F. Bianchi<sup>44</sup>, M. Bigi<sup>44</sup>, M. S. Bilenky<sup>16</sup>, P. Billoir<sup>23</sup>, M.-A. Bizouard<sup>19</sup>, D. Bloch<sup>10</sup>, M. Blume<sup>51</sup>, M. Bonesini<sup>27</sup>, W. Bonivento<sup>27</sup>, P. S. L. Booth<sup>22</sup>, A. W. Borgland<sup>4</sup>, G. Borisov<sup>38,41</sup>, C. Bosio<sup>39</sup>, O. Botner<sup>47</sup>, E. Boudinov<sup>30</sup>, B. Bouquet<sup>19</sup>, C. Bourdarios<sup>19</sup>, T. J. V. Bowcock<sup>22</sup>, M. Bozzo<sup>13</sup>, P. Branchini<sup>39</sup>, K. D. Brand<sup>35</sup>, T. Brenke<sup>51</sup>, R. A. Brenner<sup>47</sup>, C. Bricman<sup>2</sup>, R. C. A. Brown<sup>9</sup>, P. Bruckman<sup>18</sup>, J.-M. Brunet<sup>8</sup>, L. Bugge<sup>32</sup>, T. Buran<sup>32</sup>, T. Burgsmueller<sup>51</sup>, P. Buschmann<sup>51</sup>, S. Cabrera<sup>48</sup>, M. Caccia<sup>27</sup>, M. Calvi<sup>27</sup>, A. J. Camacho Rozas<sup>40</sup>, T. Camporesi<sup>9</sup>, V. Canale<sup>37</sup>, M. Canepa<sup>13</sup>, F. Cao<sup>2</sup>, F. Carena<sup>9</sup>, L. Carroll<sup>22</sup>, C. Caso<sup>13</sup>, M. V. Castillo Gimenez<sup>48</sup>, A. Cattai<sup>9</sup>, F. R. Cavallo<sup>5</sup>, V. Chabaud<sup>9</sup>, Ph. Charpentier<sup>9</sup>, L. Chaussard<sup>25</sup>, P. Checchia<sup>35</sup>, G. A. Chelkov<sup>16</sup>, M. Chen<sup>2</sup>, R. Chierici<sup>44</sup>, P. Chliapnikov<sup>41</sup>, P. Chochula<sup>7</sup>, V. Chorowicz<sup>25</sup>, V. Cindro<sup>42</sup>, P. Collins<sup>9</sup>, R. Contri<sup>13</sup>, E. Cortina<sup>48</sup>, G. Cosme<sup>19</sup>, F. Cossutti<sup>45</sup>, J.-H. Cowell<sup>22</sup>, H. B. Crawley<sup>1</sup>, D. Crennell<sup>36</sup>, G. Crosetti<sup>13</sup>, J. Cuevas Maestro<sup>33</sup>, S. Czellar<sup>15</sup>, J. Dahm<sup>51</sup>, B. Dalmagne<sup>19</sup>, M. Dam<sup>28</sup>, G. Damgaard<sup>28</sup>, P. D. Dauncey<sup>36</sup>, M. Davenport<sup>9</sup>, W. Da Silva<sup>23</sup>, A. Deghorain<sup>2</sup>, G. Della Ricca<sup>45</sup>, P. Delpierre<sup>26</sup>, N. Demaria<sup>34</sup>, A. De Angelis<sup>9</sup>, W. De Boer<sup>17</sup>, S. De Brabandere<sup>2</sup>, C. De Clercq<sup>2</sup>, C. De La Vaissiere<sup>23</sup>, B. De Lotto<sup>45</sup>, A. De Min<sup>35</sup>, L. De Paula<sup>46</sup>, H. Dijkstra<sup>9</sup>, L. Di Ciaccio<sup>37</sup>, A. Di Diodato<sup>37</sup>, A. Djannati<sup>8</sup>, J. Dolbeau<sup>8</sup>, K. Doroba<sup>50</sup>, M. Dracos<sup>10</sup>, J. Drees<sup>51</sup>, K.-A. Drees<sup>51</sup>, M. Dris<sup>31</sup>, J.-D. Durand<sup>25,9</sup>, D. Edsall<sup>1</sup>, R. Ehret<sup>17</sup>, G. Eigen<sup>4</sup>, T. Ekelof<sup>47</sup>, G. Ekspong<sup>43</sup>, M. Elsing<sup>9</sup>, J.-P. Engel<sup>10</sup>, B. Erzen<sup>42</sup>, M. Espirito Santo<sup>21</sup>, E. Falk<sup>24</sup>, G. Fanourakis<sup>11</sup>, D. Fassouliotis<sup>45</sup>, M. Feindt<sup>9</sup>, P. Ferrari<sup>27</sup>, A. Ferrer<sup>48</sup>, S. Fichet<sup>23</sup>, T. A. Filippas<sup>31</sup>, A. Firestone<sup>1</sup>, P.-A. Fischer<sup>10</sup>, H. Foeth<sup>9</sup>, E. Fokitis<sup>31</sup>, F. Fontanelli<sup>13</sup>, F. Formenti<sup>9</sup>, B. Franek<sup>36</sup>, A. G. Frodesen<sup>4</sup>, R. Fruhwirth<sup>49</sup>, F. Fulda-Quenzer<sup>19</sup>, J. Fuster<sup>48</sup>, A. Galloni<sup>22</sup>, D. Gamba<sup>44</sup>, M. Gandelman<sup>46</sup>, C. Garcia<sup>48</sup>, J. Garcia<sup>40</sup>, C. Gaspar<sup>9</sup>, U. Gasparini<sup>35</sup>, Ph. Gavellet<sup>9</sup>, E. N. Gazis<sup>31</sup>, D. Gele<sup>10</sup>, J.-P. Gerber<sup>10</sup>, L. Gerdyukov<sup>41</sup>, R. Gokheli<sup>50</sup>, B. Golob<sup>42</sup>, P. Goncalves<sup>21</sup>, G. Gopal<sup>36</sup>, L. Gorn<sup>1</sup>, M. Gorski<sup>50</sup>, Yu. Gouz<sup>44,52</sup>, V. Gracco<sup>13</sup>, E. Graziani<sup>39</sup>, C. Green<sup>22</sup>, A. Grefrath<sup>51</sup>, P. Gris<sup>38</sup>, G. Grosdidier<sup>19</sup>, K. Grzelak<sup>50</sup>, S. Gumenyuk<sup>41</sup>, M. Gunther<sup>47</sup>, J. Guy<sup>36</sup>, F. Hahn<sup>9</sup>, S. Hahn<sup>51</sup>, Z. Hajduk<sup>18</sup>, A. Hallgren<sup>47</sup>, K. Hamacher<sup>51</sup>, F. J. Harris<sup>34</sup>, V. Hedberg<sup>24</sup>, R. Henriques<sup>21</sup>, J. J. Hernandez<sup>48</sup>, P. Herquet<sup>2</sup>, H. Herr<sup>9</sup>, T. L. Hessing<sup>34</sup>, J.-M. Heuser<sup>51</sup>, E. Higon<sup>48</sup>, S.-O. Holmgren<sup>43</sup>, P. J. Holt<sup>34</sup>, D. Holthuisen<sup>30</sup>, S. Hoorelbeke<sup>2</sup>, M. Houlden<sup>22</sup>, J. Hrubec<sup>49</sup>, K. Huet<sup>2</sup>, K. Hultqvist<sup>43</sup>, J. N. Jackson<sup>22</sup>, R. Jacobsson<sup>43</sup>, P. J. Jaloche<sup>9</sup>, R. Janik<sup>7</sup>, Ch. Jarlskog<sup>24</sup>, G. Jarlskog<sup>24</sup>, P. Jarry<sup>38</sup>, B. Jean-Marie<sup>19</sup>, E. K. Johansson<sup>43</sup>, L. Jonsson<sup>24</sup>, P. Jonsson<sup>24</sup>, C. Joram<sup>9</sup>, P. Juillot<sup>10</sup>, M. Kaiser<sup>17</sup>, F. Kapusta<sup>23</sup>, K. Karafasoulis<sup>11</sup>, S. Katsanevas<sup>25</sup>, E. C. Katsoufis<sup>31</sup>, R. Keranen<sup>4</sup>, Yu. Khokhlov<sup>41</sup>, B. A. Khomenko<sup>16</sup>, N. N. Khovanski<sup>16</sup>, B. King<sup>22</sup>, N. J. Kjaer<sup>30</sup>, O. Klapp<sup>51</sup>, H. Klein<sup>9</sup>, P. Kluit<sup>30</sup>, D. Knoblach<sup>17</sup>, P. Kokkinias<sup>11</sup>, A. Konopliannikov<sup>41</sup>, M. Koratzinos<sup>9</sup>, K. Korcyl<sup>18</sup>, V. Kostoukhine<sup>41</sup>, C. Kourkoumelis<sup>3</sup>, O. Kouznetsov<sup>13,16</sup>, M. Kramer<sup>49</sup>, C. Kreuter<sup>9</sup>, I. Kronkvist<sup>24</sup>, Z. Kruminer<sup>16</sup>, W. Krupinski<sup>18</sup>, P. Kubinec<sup>7</sup>, W. Kucewicz<sup>18</sup>, K. Kurvinen<sup>15</sup>, C. Lacasta<sup>9</sup>, I. Laktineh<sup>25</sup>, J. W. Lamsa<sup>1</sup>, L. Lanteri<sup>45</sup>, D. W. Lane<sup>1</sup>, P. Langefeld<sup>51</sup>, J.-P. Laugier<sup>38</sup>, R. Lauhakangas<sup>15</sup>, G. Leder<sup>49</sup>, F. Ledroit<sup>14</sup>, V. Lefebvre<sup>2</sup>, C. K. Legan<sup>1</sup>, A. Leisos<sup>11</sup>, R. Leitner<sup>29</sup>, J. Lemonne<sup>2</sup>, G. Lenzen<sup>51</sup>, V. Lepeltier<sup>19</sup>, T. Lesiak<sup>18</sup>, J. Libby<sup>34</sup>, D. Liko<sup>9</sup>, A. Lipniacka<sup>43</sup>, I. Lippi<sup>35</sup>, B. Loerstad<sup>24</sup>, J. G. Loken<sup>34</sup>, J. M. Lopez<sup>40</sup>, D. Loukas<sup>11</sup>, P. Lutz<sup>38</sup>, L. Lyons<sup>34</sup>, J. MacNaughton<sup>49</sup>, G. Maehlum<sup>17</sup>, J. R. Mahon<sup>6</sup>, A. Maio<sup>21</sup>, T. G. M. Malmgren<sup>43</sup>, V. Malychev<sup>16</sup>, F. Mandl<sup>49</sup>, J. Marco<sup>40</sup>, R. Marco<sup>40</sup>, B. Marechal<sup>46</sup>, M. Margoni<sup>35</sup>, J.-C. Marin<sup>9</sup>, C. Mariotti<sup>9</sup>, A. Markou<sup>11</sup>, C. Martinez-Rivero<sup>33</sup>, F. Martinez-Vidal<sup>48</sup>, S. Marti i Garcia<sup>22</sup>, F. Matorras<sup>40</sup>, C. Matteuzzi<sup>27</sup>, G. Matthiae<sup>37</sup>, M. Mazzucato<sup>35</sup>, M. Mc Cubbin<sup>22</sup>, R. Mc Kay<sup>1</sup>, R. Mc Nulty<sup>9</sup>, G. Mc Pherson<sup>22</sup>, J. Medbo<sup>47</sup>, C. Meroni<sup>27</sup>, S. Meyer<sup>17</sup>, W. T. Meyer<sup>1</sup>, M. Michelotto<sup>35</sup>, E. Migliore<sup>44</sup>, L. Mirabito<sup>25</sup>, W. A. Mitaroff<sup>49</sup>, U. Mjoernmark<sup>24</sup>, T. Moa<sup>43</sup>, R. Moeller<sup>28</sup>, K. Moenig<sup>9</sup>, M. R. Monge<sup>13</sup>, P. Moretti<sup>13</sup>, H. Mueller<sup>17</sup>, K. Muenich<sup>51</sup>, M. Mulders<sup>30</sup>, L. M. Mundim<sup>6</sup>, W. J. Murray<sup>36</sup>, B. Muryn<sup>14,18</sup>, G. Myatt<sup>34</sup>, T. Myklebust<sup>32</sup>, F. Naraghi<sup>14</sup>, F. L. Navarria<sup>5</sup>, S. Navas<sup>48</sup>, K. Nawrocki<sup>50</sup>, P. Negri<sup>27</sup>, S. Nemecek<sup>12</sup>, W. Neumann<sup>51</sup>, N. Neumeister<sup>49</sup>, R. Nicolaidou<sup>3</sup>, B. S. Nielsen<sup>28</sup>, M. Nieuwenhuizen<sup>30</sup>, V. Nikolaenko<sup>10</sup>, M. Nikolenko<sup>10,16</sup>, P. Niss<sup>43</sup>, A. Nomerotski<sup>35</sup>, A. Normand<sup>22</sup>, A. Nygren<sup>24</sup>, W. Oberschulte-Beckmann<sup>17</sup>, V. Obraztsov<sup>41</sup>, A. G. Olshevski<sup>16</sup>, A. Onofre<sup>21</sup>, R. Orava<sup>15</sup>, G. Orazi<sup>10</sup>, K. Osterberg<sup>15</sup>, A. Ouraou<sup>38</sup>, P. Paganini<sup>19</sup>, M. Paganoni<sup>9,27</sup>, R. Pain<sup>23</sup>, H. Palka<sup>18</sup>, Th. D. Papadopoulou<sup>31</sup>, K. Papageorgiou<sup>11</sup>, L. Pape<sup>9</sup>, C. Parkes<sup>34</sup>, F. Parodi<sup>13</sup>, U. Parzefall<sup>22</sup>, A. Passeri<sup>39</sup>, M. Pegoraro<sup>35</sup>, L. Peralta<sup>21</sup>, H. Pernegger<sup>49</sup>, A. Perrotta<sup>5</sup>, C. Petridou<sup>45</sup>, A. Petrolini<sup>13</sup>, H. T. Phillips<sup>36</sup>, G. Piana<sup>13</sup>, F. Pierre<sup>38</sup>, M. Pimenta<sup>21</sup>, T. Podobnik<sup>34</sup>, O. Podobrin<sup>9</sup>, M. E. Pol<sup>6</sup>, G. Polok<sup>18</sup>, P. Poropat<sup>45</sup>, V. Pozdniakov<sup>16</sup>, P. Privitera<sup>37</sup>, N. Pukhaeva<sup>16</sup>, A. Pullia<sup>27</sup>, D. Radojicic<sup>34</sup>, S. Ragazzi<sup>27</sup>, H. Rahmani<sup>31</sup>, J. Rames<sup>12</sup>, P. N. Ratoff<sup>20</sup>, A. L. Read<sup>32</sup>, M. Reale<sup>51</sup>, P. Rebecchi<sup>9</sup>, N. G. Redaelli<sup>27</sup>, M. Regler<sup>49</sup>, D. Reid<sup>9</sup>, R. Reinhardt<sup>51</sup>, P. B. Renton<sup>34</sup>, L. K. Resvanis<sup>3</sup>, F. Richard<sup>19</sup>, J. Ridky<sup>12</sup>, G. Rinaudo<sup>44</sup>, O. Rohne<sup>32</sup>, A. Romero<sup>44</sup>, P. Ronchese<sup>35</sup>, L. Roos<sup>23</sup>, E. I. Rosenberg<sup>1</sup>, P. Rosinsky<sup>7</sup>, P. Roudeau<sup>19</sup>, T. Rovelli<sup>5</sup>, V. Ruhlmann-Kleider<sup>38</sup>, A. Ruiz<sup>40</sup>, K. Rybicki<sup>18</sup>, H. Saarikko<sup>15</sup>, Y. Sacquin<sup>38</sup>, A. Sadovsky<sup>16</sup>, G. Sajot<sup>14</sup>, J. Salt<sup>48</sup>, M. Sannino<sup>13</sup>, H. Schneider<sup>17</sup>, U. Schwickerath<sup>17</sup>, M. A. E. Schyns<sup>51</sup>, G. Sciolla<sup>44</sup>, F. Scuri<sup>45</sup>, P. Seager<sup>20</sup>, Y. Sedykh<sup>16</sup>, A. M. Segar<sup>34</sup>, A. Seitz<sup>17</sup>, R. Sekulin<sup>36</sup>, L. Serbelloni<sup>37</sup>, R. C. Shellard<sup>6</sup>, A. Sheridan<sup>22</sup>, I. Siccama<sup>30</sup>, P. Siegrist<sup>9,38</sup>, R. Silvestre<sup>38</sup>, F. Simonetto<sup>35</sup>, A. N. Sisakian<sup>16</sup>, T. B. Skaali<sup>32</sup>, G. Smadja<sup>25</sup>, N. Smirnov<sup>41</sup>, O. Smirnova<sup>24</sup>, G. R. Smith<sup>36</sup>, O. Solovianov<sup>41</sup>, R. Sosnowski<sup>50</sup>, D. Souza-Santos<sup>6</sup>, T. Spassov<sup>21</sup>, E. Spiriti<sup>39</sup>, P. Sponholz<sup>51</sup>, S. Squarcia<sup>13</sup>, D. Stampfer<sup>9</sup>, C. Stanescu<sup>39</sup>, S. Stanic<sup>42</sup>, S. Stapnes<sup>32</sup>, I. Stavitski<sup>35</sup>, K. Stevenson<sup>34</sup>, A. Stocchi<sup>19</sup>, J. Strauss<sup>49</sup>, R. Strub<sup>10</sup>, B. Stugu<sup>4</sup>, M. Szczekowski<sup>50</sup>, M. Szeptycka<sup>50</sup>, T. Tabarelli<sup>27</sup>, J. P. Tavernet<sup>23</sup>, E. Tcherniaev<sup>41</sup>, O. Tchikilev<sup>41</sup>, F. Tegenfeldt<sup>47</sup>, F. Terranova<sup>27</sup>, J. Thomas<sup>34</sup>, A. Tilquin<sup>26</sup>, J. Timmermans<sup>30</sup>

L.G.Tkatchev<sup>16</sup>, T.Todorov<sup>10</sup>, S.Todorova<sup>10</sup>, D.Z.Toet<sup>30</sup>, A.Tomaradze<sup>2</sup>, B.Tome<sup>21</sup>, A.Tonazzo<sup>27</sup>, L.Tortora<sup>39</sup>, G.Transtomer<sup>24</sup>, D.Treille<sup>9</sup>, G.Tristram<sup>8</sup>, A.Trombini<sup>19</sup>, C.Troncon<sup>27</sup>, A.Tsirou<sup>9</sup>, M-L.Turluer<sup>38</sup>, I.A.Tyapkin<sup>16</sup>, M.Tyndel<sup>36</sup>, S.Tzamaras<sup>11</sup>, B.Ueberschaer<sup>51</sup>, O.Ullaland<sup>9</sup>, V.Uvarov<sup>41</sup>, G.Valenti<sup>5</sup>, E.Vallazza<sup>45</sup>, C.Vander Velde<sup>2</sup>, G.W.Van Apeldoorn<sup>30</sup>, P.Van Dam<sup>30</sup>, W.K.Van Doninck<sup>2</sup>, J.Van Eldik<sup>30</sup>, A.Van Lysebetten<sup>2</sup>, N.Vassilopoulos<sup>34</sup>, G.Vegni<sup>27</sup>, L.Ventura<sup>35</sup>, W.Venus<sup>36</sup>, F.Verbeure<sup>2</sup>, M.Verlato<sup>35</sup>, L.S.Vertogradov<sup>16</sup>, D.Vilanova<sup>38</sup>, P.Vincent<sup>25</sup>, L.Vitale<sup>45</sup>, A.S.Vodopyanov<sup>16</sup>, V.Vrba<sup>12</sup>, H.Wahlen<sup>51</sup>, C.Walck<sup>43</sup>, F.Waldner<sup>45</sup>, C.Weiser<sup>17</sup>, A.M.Wetherell<sup>9</sup>, D.Wicke<sup>51</sup>, J.H.Wickens<sup>2</sup>, M.Wielers<sup>17</sup>, G.R.Wilkinson<sup>9</sup>, W.S.C.Williams<sup>34</sup>, M.Winter<sup>10</sup>, M.Witek<sup>18</sup>, T.Wlodek<sup>19</sup>, J.Yi<sup>1</sup>, K.Yip<sup>34</sup>, O.Yushchenko<sup>41</sup>, F.Zach<sup>25</sup>, A.Zaitsev<sup>41</sup>, A.Zalewska<sup>9</sup>, P.Zalewski<sup>50</sup>, D.Zavrtanik<sup>42</sup>, E.Zevgolatakos<sup>11</sup>, N.I.Zimin<sup>16</sup>, G.C.Zucchelli<sup>43</sup>, G.Zumerle<sup>35</sup>

<sup>1</sup>Department of Physics and Astronomy, Iowa State University, Ames IA 50011-3160, USA

<sup>2</sup>Physics Department, Univ. Instelling Antwerpen, Universiteitsplein 1, B-2610 Wilrijk, Belgium and IIHE, ULB-VUB, Pleinlaan 2, B-1050 Brussels, Belgium

and Faculté des Sciences, Univ. de l'Etat Mons, Av. Maistriau 19, B-7000 Mons, Belgium

<sup>3</sup>Physics Laboratory, University of Athens, Solonos Str. 104, GR-10680 Athens, Greece

<sup>4</sup>Department of Physics, University of Bergen, Allégaten 55, N-5007 Bergen, Norway

<sup>5</sup>Dipartimento di Fisica, Università di Bologna and INFN, Via Irnerio 46, I-40126 Bologna, Italy

<sup>6</sup>Centro Brasileiro de Pesquisas Físicas, rua Xavier Sigaud 150, RJ-22290 Rio de Janeiro, Brazil and Depto. de Física, Pont. Univ. Católica, C.P. 38071 RJ-22453 Rio de Janeiro, Brazil

and Inst. de Física, Univ. Estadual do Rio de Janeiro, rua São Francisco Xavier 524, Rio de Janeiro, Brazil

<sup>7</sup>Comenius University, Faculty of Mathematics and Physics, Mlynska Dolina, SK-84215 Bratislava, Slovakia

<sup>8</sup>Collège de France, Lab. de Physique Corpusculaire, IN2P3-CNRS, F-75231 Paris Cedex 05, France

<sup>9</sup>CERN, CH-1211 Geneva 23, Switzerland

<sup>10</sup>Institut de Recherches Subatomiques, IN2P3 - CNRS/ULP - BP20, F-67037 Strasbourg Cedex, France

<sup>11</sup>Institute of Nuclear Physics, N.C.S.R. Demokritos, P.O. Box 60228, GR-15310 Athens, Greece

<sup>12</sup>FZU, Inst. of Physics of the C.A.S. High Energy Physics Division, Na Slovance 2, 180 40, Praha 8, Czech Republic

<sup>13</sup>Dipartimento di Fisica, Università di Genova and INFN, Via Dodecaneso 33, I-16146 Genova, Italy

<sup>14</sup>Institut des Sciences Nucléaires, IN2P3-CNRS, Université de Grenoble 1, F-38026 Grenoble Cedex, France

<sup>15</sup>Helsinki Institute of Physics, HIP, P.O. Box 9, FIN-00014 Helsinki, Finland

<sup>16</sup>Joint Institute for Nuclear Research, Dubna, Head Post Office, P.O. Box 79, 101 000 Moscow, Russian Federation

<sup>17</sup>Institut für Experimentelle Kernphysik, Universität Karlsruhe, Postfach 6980, D-76128 Karlsruhe, Germany

<sup>18</sup>Institute of Nuclear Physics and University of Mining and Metallurgy, Ul. Kawiory 26a, PL-30055 Krakow, Poland

<sup>19</sup>Université de Paris-Sud, Lab. de l'Accélérateur Linéaire, IN2P3-CNRS, Bât. 200, F-91405 Orsay Cedex, France

<sup>20</sup>School of Physics and Chemistry, University of Lancaster, Lancaster LA1 4YB, UK

<sup>21</sup>LIP, IST, FCUL - Av. Elias Garcia, 14-1º, P-1000 Lisboa Codex, Portugal

<sup>22</sup>Department of Physics, University of Liverpool, P.O. Box 147, Liverpool L69 3BX, UK

<sup>23</sup>LPNHE, IN2P3-CNRS, Universités Paris VI et VII, Tour 33 (RdC), 4 place Jussieu, F-75252 Paris Cedex 05, France

<sup>24</sup>Department of Physics, University of Lund, Sölvegatan 14, S-22363 Lund, Sweden

<sup>25</sup>Université Claude Bernard de Lyon, IPNL, IN2P3-CNRS, F-69622 Villeurbanne Cedex, France

<sup>26</sup>Univ. d'Aix - Marseille II - CPP, IN2P3-CNRS, F-13288 Marseille Cedex 09, France

<sup>27</sup>Dipartimento di Fisica, Università di Milano and INFN, Via Celoria 16, I-20133 Milan, Italy

<sup>28</sup>Niels Bohr Institute, Blegdamsvej 17, DK-2100 Copenhagen 0, Denmark

<sup>29</sup>NC, Nuclear Centre of MFF, Charles University, Areal MFF, V Holesovickach 2, 180 00, Praha 8, Czech Republic

<sup>30</sup>NIKHEF, Postbus 41882, NL-1009 DB Amsterdam, The Netherlands

<sup>31</sup>National Technical University, Physics Department, Zografou Campus, GR-15773 Athens, Greece

<sup>32</sup>Physics Department, University of Oslo, Blindern, N-1000 Oslo 3, Norway

<sup>33</sup>Dpto. Física, Univ. Oviedo, Avda. Calvo Sotelo, S/N-33007 Oviedo, Spain, (CICYT-AEN96-1681)

<sup>34</sup>Department of Physics, University of Oxford, Keble Road, Oxford OX1 3RH, UK

<sup>35</sup>Dipartimento di Fisica, Università di Padova and INFN, Via Marzolo 8, I-35131 Padua, Italy

<sup>36</sup>Rutherford Appleton Laboratory, Chilton, Didcot OX11 0QX, UK

<sup>37</sup>Dipartimento di Fisica, Università di Roma II and INFN, Tor Vergata, I-00173 Rome, Italy

<sup>38</sup>CEA, DAPNIA/Service de Physique des Particules, CE-Saclay, F-91191 Gif-sur-Yvette Cedex, France

<sup>39</sup>Istituto Superiore di Sanità, Ist. Naz. di Fisica Nucl. (INFN), Viale Regina Elena 299, I-00161 Rome, Italy

<sup>40</sup>Instituto de Física de Cantabria (CSIC-UC), Avda. los Castros, S/N-39006 Santander, Spain, (CICYT-AEN96-1681)

<sup>41</sup>Inst. for High Energy Physics, Serpukov P.O. Box 35, Protvino, (Moscow Region), Russian Federation

<sup>42</sup>J. Stefan Institute, Jamova 39, SI-1000 Ljubljana, Slovenia and Department of Astroparticle Physics, School of Environmental Sciences, Kostanjevska 16a, Nova Gorica, SI-5000 Slovenia, and Department of Physics, University of Ljubljana, SI-1000 Ljubljana, Slovenia

<sup>43</sup>Fysikum, Stockholm University, Box 6730, S-113 85 Stockholm, Sweden

<sup>44</sup>Dipartimento di Fisica Sperimentale, Università di Torino and INFN, Via P. Giuria 1, I-10125 Turin, Italy

<sup>45</sup>Dipartimento di Fisica, Università di Trieste and INFN, Via A. Valerio 2, I-34127 Trieste, Italy and Istituto di Fisica, Università di Udine, I-33100 Udine, Italy

<sup>46</sup>Univ. Federal do Rio de Janeiro, C.P. 68528 Cidade Univ., Ilha do Fundão BR-21945-970 Rio de Janeiro, Brazil

<sup>47</sup>Department of Radiation Sciences, University of Uppsala, P.O. Box 535, S-751 21 Uppsala, Sweden

<sup>48</sup>IFIC, Valencia-CSIC, and D.F.A.M.N., U. de Valencia, Avda. Dr. Moliner 50, E-46100 Burjassot (Valencia), Spain

<sup>49</sup>Institut für Hochenergiephysik, Österr. Akad. d. Wissensch., Nikolsdorfergasse 18, A-1050 Vienna, Austria

<sup>50</sup>Inst. Nuclear Studies and University of Warsaw, Ul. Hoza 69, PL-00681 Warsaw, Poland

<sup>51</sup>Fachbereich Physik, University of Wuppertal, Postfach 100 127, D-42097 Wuppertal, Germany

<sup>52</sup>On leave of absence from IHEP Serpukhov

# 1 Introduction

In the Standard Model,  $B_d^0 - \overline{B}_d^0$  mixing is a direct consequence of second order weak interactions. Starting with a  $B_d^0$  meson produced at time  $t=0$ , the probability,  $\mathcal{P}$ , to observe a  $B_d^0$  decaying at the proper time  $t$  can be written, neglecting effects from CP violation:

$$\mathcal{P}(B_d^0 \rightarrow B_d^0) = \frac{\Gamma_d}{2} e^{-\Gamma_d t} \left\{ \cosh\left(\frac{\Delta\Gamma_d}{2} t\right) + \cos(\Delta m_d t) \right\} \quad (1)$$

where  $\Gamma_d = \frac{\Gamma_d^H + \Gamma_d^L}{2}$ ,  $\Delta\Gamma_d = \Gamma_d^H - \Gamma_d^L$ ,  $\Delta m_d = m_d^H - m_d^L$ , and  $L$  and  $H$  denote the light and heavy physical states respectively. The oscillation frequency gives a direct measurement of the mass difference between the two physical states. The Standard Model predicts that  $\Delta\Gamma_d \ll \Delta m_d$ , in which case the above expression simplifies to :

$$\mathcal{P}_{B_d^0}^{unmix.} = \mathcal{P}(B_d^0 \rightarrow B_d^0) = \Gamma_d e^{-\Gamma_d t} \cos^2\left(\frac{\Delta m_d t}{2}\right) \quad (2)$$

and similarly:

$$\mathcal{P}_{B_d^0}^{mix.} = \mathcal{P}(B_d^0 \rightarrow \overline{B}_d^0) = \Gamma_d e^{-\Gamma_d t} \sin^2\left(\frac{\Delta m_d t}{2}\right) \quad (3)$$

Keeping only the dominant top quark contribution,  $\Delta m_d$  can be expressed in terms of Standard Model parameters [1]:

$$\Delta m_d = \frac{G_F^2}{6\pi^2} |V_{tb}|^2 |V_{td}|^2 \overline{m}_t^2 m_{B_d} f_{B_d}^2 B_{B_d} \eta_B F(x_t). \quad (4)$$

In this expression  $G_F$  is the Fermi coupling constant,  $V_{tb}$  and  $V_{td}$  are elements of the CKM matrix,  $f_{B_d}$  and  $B_{B_d}$  are the pseudoscalar decay constant and the bag factor respectively and are of non-perturbative origin,  $\eta_B$  represents the short distance QCD corrections to the relevant box diagrams, and  $F(x_t)$ , with  $x_t = \frac{\overline{m}_t^2}{m_W^2}$ , results from the evaluation of the box diagram and is expressed by the following formula:

$$F(x_t) = \frac{1}{4} + \frac{9}{4} \frac{1}{1-x_t} - \frac{3}{2} \frac{1}{(1-x_t)^2} - \frac{3}{2} \frac{x_t^2}{(1-x_t)^3} \ln x_t. \quad (5)$$

The present uncertainty on the top mass measurement,  $m_t = 175 \pm 9 \text{ GeV}/c^2$  [2], gives an 11% uncertainty on the evaluation of  $\Delta m_d$ . The scale for the evaluation of perturbative corrections entering into  $\eta_B$  and of the running of the  $t$  quark mass, have to be defined in a consistent way. The measured value of the pole quark mass has to be corrected downward by  $7 \pm 1 \text{ GeV}/c^2$  [3]. In the  $\overline{\text{MS}}$  scheme the following values have been obtained:

$$\overline{m}_t = 168 \pm 9 \text{ GeV}/c^2, \quad \eta_B = 0.55 \pm 0.01 \quad (6)$$

The largest theoretical uncertainties originate in the evaluation of the parameters  $f_{B_d}$  and  $B_{B_d}$  and from  $|V_{td}|$  ( $V_{tb}$  is close to unity, assuming the unitarity of the CKM matrix). Precise measurements of  $\Delta m_d$  will bring a constraint on these parameters and, if progress is accomplished in lattice QCD evaluations of  $f_{B_d}$  and  $B_{B_d}$ ,  $|V_{td}|$  can be determined.

The time integrated mixing probability,

$$\chi_d = \frac{x_d^2}{2(1+x_d^2)} \quad (7)$$

with  $x_d = \frac{\Delta m_d}{\Gamma_d}$ , has been measured at the  $\Upsilon(4S)$  [4] and  $\bar{\chi} = f_d \chi_d + f_s \chi_s$  where  $f_d$  and  $f_s$  are the  $B_d$  and  $B_s$  fractions in  $b$  jets, has been measured at LEP and at hadron

colliders [5]. Numerous measurements of time dependent oscillations of  $B_d^0$  mesons, which determine  $\Delta m_d$  directly, have been made at LEP [6].

The present measurements of  $\Delta m_d$  were obtained using 3.2 million hadronic  $Z^0$  decays registered by DELPHI between 1991 and 1994. The principle of the method is that, after dividing the charged and neutral particles from a  $Z^0$  decay into two hemispheres separated by the plane transverse to the sphericity axis, a *production sign* is defined in one hemisphere which is correlated with the  $b/\bar{b}$  nature of the initial quark at the production point, while in the other hemisphere *a)* the decay time of the B hadron candidate is evaluated, and *b)* a *decay sign* is defined, correlated to the  $B/\bar{B}$  nature of the decaying hadron.

In the analyses reported here, either the charge of a high  $p_t$  lepton, or the measurement of the momentum-weighted sum of the charges of the particles present in the hemisphere (the hemisphere-charge  $Q_{hem}$ ), is used to define the production sign. The decay sign is obtained either from the sign of another high  $p_t$  lepton, or from the charge of a  $D^{*\pm}$ . The latter gives, in addition, an enrichment in  $B_d^0$  of the selected event sample.

Two types of analysis are presented. In the analysis based on the exclusive reconstruction of  $D^{*\pm}$  decays, the decay distance of the  $D^0$  and the central value of the B momentum are used to evaluate the B meson decay time. The other three analyses are based on more inclusive reconstructions of semileptonic B decay channels, and they all use an algorithm that has been developed to measure both the position of the B decay vertex and the B momentum from the lepton and all other particles present in the same jet as the lepton.

Sect. 2 describes the components of the DELPHI detector which are important for this analysis. Sect. 3 explains the event selection and Monte Carlo simulation. The measurement of the  $b$  quark charge using the jet-charge is described in Sect. 4. Sect. 5 gives the measurements of  $\Delta m_d$  from the exclusive reconstruction of  $D^{*\pm}$  decays. Sect. 6 presents the three inclusive measurements of  $\Delta m_d$ . Finally, the combined result is given in Sect. 7.

## 2 The DELPHI detector

The events used in this analysis were recorded with the DELPHI detector at LEP running near the  $Z^0$  peak. The performance of the detector is described in [7]. The relevant parts for lepton identification are the muon chambers and the electromagnetic calorimeters. The Vertex Detector (VD) is used in combination with the central tracking devices to measure precisely the charged particle trajectories close to the beam interaction region.

The DELPHI reference frame is defined with  $z$  along the  $e^-$  beam,  $x$  towards the centre of LEP, and  $y$  upwards. The angular coordinates are the polar angle  $\theta$ , measured from the  $z$  axis, and the azimuth angle  $\phi$ , measured from the  $x$ -axis.  $R$  is the radial distance from the  $z$ -axis.

The muon chambers are drift chambers located at the periphery of DELPHI. The barrel part ( $-0.63 < \cos\theta < 0.63$ ) is composed of three sets of modules, each of two active layers, that give  $z$  and  $R\phi$  coordinates. In the forward part, two layers of two planes give the  $x$  and  $y$  coordinates in the transverse plane. The precision of these detectors has to be taken into account for muon identification: it has been measured to be  $\pm 1$  cm in  $z$  and  $\pm 0.2$  cm in  $R\phi$  for the barrel part, and  $\pm 0.4$  cm for each of the two coordinates given by the forward part. The number of absorption lengths in front of the

muon chambers, which largely determines the hadron contamination, is approximately 8 for  $\theta = 90^\circ$ .

Electrons are absorbed in the electromagnetic calorimeters. The High density Projection Chamber (HPC), which covers the angular region used in this analysis, provides three dimensional information on electromagnetic showers. It has 18 radiation lengths thickness for  $\theta = 90^\circ$ .

During the first part of the data taking period (1991 to 1993), the Vertex Detector [8] consisted of three concentric shells of silicon strip detectors, at average radii of 6.3, 9 and 11 cm, that measured the coordinates of charged particle tracks in the transverse plane with respect to the beam direction ( $R\phi$ ) with a precision of  $\pm 8 \mu\text{m}$ . The association of this detector with the central tracking system of DELPHI, consisting of the Time Projection Chamber (TPC) and the Inner and Outer Detectors, gave  $\sqrt{20^2 + (65/p)^2} \mu\text{m}$  ( $p$  in  $\text{GeV}/c$  units) precision on the transverse impact parameter of charged particles with respect to the primary vertex. For the data registered in 1994, the inner and outer shells of the VD were equipped with double-sided detectors, providing additional accurate measurements of the charged particle trajectories along the beam direction ( $z$ ). The single hit precision of the  $z$  coordinate is a function of the incident angle of the track, reaching a value of  $\pm 9 \mu\text{m}$  for tracks perpendicular to the modules.

The 192 sense wires of the TPC measure the specific energy loss,  $dE/dx$ , of charged particles, as the 80% truncated mean of the amplitudes of the wire signals, with a minimum requirement of 30 wires. This  $dE/dx$  measurement is available for 75% of charged particles in hadronic jets, with a precision which was measured to be  $\pm 6.7\%$  in the momentum range  $4 < p < 25 \text{ GeV}/c$ . It was used in electron identification.

To identify kaons with momenta between 3 and 15  $\text{GeV}/c$  (this range corresponds to the typical momentum for kaons from a B decay), the gas radiator of the barrel Ring Imaging Cherenkov detector (RICH) [9] is used: below 8.5  $\text{GeV}/c$ , it works in the *veto* mode (kaons and protons give no Cherenkov photons and are thus distinguished from pions and leptons, but not from each other); above this threshold, kaons are distinguished from all other charged particles by measuring the radius of the ring of detected Cherenkov photons.

### 3 Event selection and simulation

Each event was divided into two hemispheres separated by the plane transverse to the sphericity axis. Hadronic decays of the  $Z^0$  were selected by requiring the total energy of the charged particles in each hemisphere to exceed 3 GeV (assuming all charged particles to be pions), the total energy of the charged particles to exceed 15 GeV, and at least 5 charged particles with momenta above 0.2  $\text{GeV}/c$ . A clustering analysis based on the JETSET algorithm LUCLUS with default parameters [10] was used to define jets, using both charged and neutral particles. These jets were used to compute the  $p_t$  of each particle in the event, defined as its momentum transverse to the axis of the rest of the jet it belonged to, after removing the particle from its jet.

Simulated events were generated using the JETSET 7.3 program [10]. Semileptonic B hadron decays were simulated using the ISGW model [11]. These events were followed through the full simulation of the DELPHI detector (DELSIM) [7].

The values of the parameters which are relevant for the four analyses of this paper are given in Tab. 1.

## 4 $b(\bar{b})$ tagging using the hemisphere charge

The mean charge of an event hemisphere was defined as

$$Q_{hem} = \frac{\sum_{i=1}^n q_i (\vec{p}_i \cdot \vec{e}_s)^\kappa}{\sum_{i=1}^n (\vec{p}_i \cdot \vec{e}_s)^\kappa}, \quad (8)$$

where  $q_i$  and  $\vec{p}_i$  are the charge and the momentum of the particle  $i$  respectively,  $\vec{e}_s$  is the unit vector along the sphericity axis,  $\kappa$  is an adjustable parameter which was put equal to 0.6, and the sum is extended over all charged particles in the hemisphere. The correctness of the  $b$  charge determination depends on the  $b$  hadron type and, for  $B_d$  and  $B_s$  mesons, it is also sensitive to the time-integrated value of the mixing.

The value chosen for  $\kappa$  corresponds to the best separation between the  $Q_{hem}$  distributions of the  $b$  and  $\bar{b}$  quarks according to the simulation. For pure  $b\bar{b}$  events, if a  $\bar{b}$  candidate is selected by requiring  $Q_{hem} > 0.0$ , the fraction of correct tags,  $\epsilon_b^Q$ , is  $(64.2 \pm 0.2)\%$ . In order to improve  $\epsilon_b^Q$ , events were selected by requiring  $|Q_{hem}|$  to be larger than a certain smallest value  $\Delta Q_{hem}$ . If  $f_{tag}$  is the fraction of tagged  $b$  or  $\bar{b}$  events after this requirement, the statistical significance of a signal from oscillations is proportional to  $\sqrt{f_{tag}} \times (2\epsilon_b^Q - 1)$ , and was found using simulated events to be optimized for a value of  $\Delta Q_{hem} = 0.1$ , yielding  $\epsilon_b^Q = 68.8\%$  and  $f_{tag} = 67.5\%$ . Therefore, this value of  $\Delta Q_{hem}$  was used.

The value of the tagging purity,  $\epsilon_b^Q$ , depends on details of the hadronization of  $b$  quarks, of B hadron decay properties and production rates, and of the capabilities of the charged particle reconstruction algorithm. In order to reduce systematic uncertainties,  $\epsilon_b^Q$  was measured, simultaneously with  $\Delta m_d$ , directly from the data. For non- $b\bar{b}$  events, there is no genuine oscillating component. The fractions of these events classified as mixed,  $\epsilon_c^{mix}$  and  $\epsilon_h^{mix}$  corresponding to charm and light quark flavours respectively, were determined by simulation. The uncertainties on these parameters were obtained by comparing the values of the tagging purities in  $b$  events expected from the simulation and measured in the data.

## 5 Measurement of $\Delta m_d$ in events with an exclusively reconstructed $D^{*\pm}$

This measurement is based on the reconstruction of a  $D^{*\pm}$ . The measurement of  $B_d^0 - \bar{B}_d^0$  mixing was performed by correlating *a*) the sign of the  $D^{*\pm}$  charge, which tags the B flavour at the time of decay (since  $D^{*-}$  in these events are mainly produced from  $B_d^0$  and  $D^{*+}$  from  $\bar{B}_d^0$ ), with *b*) the mean hemisphere charge in the hemisphere opposite to the  $D^{*\pm}$ . If the  $B^0$  meson decaying into a  $D^{*\pm}$  has oscillated, the  $D^{*\pm}$  charge and the charge  $Q_{hem}$  of the hemisphere opposite to the  $D^{*\pm}$  should be of unlike sign; if it has not oscillated, they should be of like sign.

### 5.1 Event selection

The  $D^{*\pm}$  candidates were selected by reconstructing the decay chain  $D^{*+} \rightarrow D^0 \pi^+$  followed by  $D^0 \rightarrow K^- \pi^+$ ,  $D^0 \rightarrow K^- \pi^+ \pi^0$ , or  $D^0 \rightarrow K^- \pi^+ \pi^+ \pi^-$ <sup>†</sup>. The selection criteria relied mainly on the small mass difference between  $D^{*+}$  and  $D^0$  mesons.

<sup>†</sup>Charge conjugates of all the decays are always implicitly included.

The decays  $D^0 \rightarrow K^- \pi^+$  and  $K^- \pi^+ \pi^0$  were reconstructed by combining all pairs of particles of opposite charge where each particle had a momentum greater than 1 GeV/c. The invariant mass of the pair was calculated assigning in turn the kaon or the pion mass to each of the particles. The  $\pi^0$  in the  $D^0 \rightarrow K^- \pi^+ \pi^0$  decay was not reconstructed.

The decay  $D^0 \rightarrow K^- \pi^+ \pi^+ \pi^-$  was reconstructed by analyzing all four track combinations of zero total charge. The kaon mass hypothesis was assigned in turn to each charged particle, and a minimum momentum of 2 GeV/c was required for the kaon and of 0.4 GeV/c for the pions.

Then, all other pion candidates with momentum between 0.4 GeV/c and 4.5 GeV/c and with a charge opposite to the kaon charge were considered for a  $D^{*\pm}$  candidate.

The ratio of the  $D^{*\pm}$  energy to the beam energy ( $X_{D^*} = E_{D^*}/E_{beam}$ ) was required to be between 0.15 and 0.50. The lower bound was chosen to reject a large part of the combinatorial background, while the upper bound was selected to reject a large part of the  $c\bar{c}$  background, since  $D^{*\pm}$  mesons produced in  $b\bar{b}$  events have a softer energy spectrum than those produced in  $c\bar{c}$  events. About 50% of the  $D^{*\pm}$  coming from  $c\bar{c}$  are rejected by requiring  $X_{D^*} < 0.5$ , whereas about 85% of the  $D^{*\pm}$  from  $b\bar{b}$  are retained.

Further selection criteria were applied which depend on the specific decay channel.

- $D^0 \rightarrow K^- \pi^+$ .

The mass of the  $D^0$  candidates had to be between 1.79 and 1.94 GeV/c<sup>2</sup> for  $X_{D^*} > 0.25$  or between 1.82 and 1.90 GeV/c<sup>2</sup> for  $0.15 < X_{D^*} < 0.25$ . To reduce the combinatorial background, the cosine of the angle  $\theta^*$  between the  $D^0$  flight direction in the laboratory and the kaon direction in the  $D^0$  rest frame had to exceed  $-0.8$  for  $0.25 < X_{D^*} < 0.50$  and  $-0.6$  for  $0.15 < X_{D^*} < 0.25$ . Tighter requirements on the  $D^0$  mass and on  $\cos \theta^*$  were necessary in  $X_{D^*}$  range  $0.15 < X_{D^*} < 0.25$ , because of the larger combinatorial background. The distribution of the mass difference  $\Delta M = M(K^- \pi^+ \pi^+) - M(K^- \pi^+)$  obtained after applying the above selection criteria is shown in Fig. 1a. In the range of  $\Delta M$  between 0.1445 and 0.1465 GeV/c<sup>2</sup>, 3409 events are observed of which about 70% are expected to be true  $D^{*\pm}$ .

- $D^0 \rightarrow K^- \pi^+ \pi^0$ .

Tighter selection criteria were applied than for the  $D^0 \rightarrow K^- \pi^+$  channel since, because of the worse mass resolution due to the missing  $\pi^0$ , a greater combinatorial background is present.  $X_{D^*}$  had to be greater than 0.25, where  $E_{D^*}$  was obtained from the sum of the kaon and charged pion energies. The invariant mass distribution of the  $K^- \pi^+$  candidates does not peak at the nominal  $D^0$  mass value, because the  $\pi^0$  is not reconstructed. Instead, a broad peak in the invariant mass is observed around 1.60 GeV/c<sup>2</sup>, which corresponds to the kinematical configuration with low energy  $\pi^0$ 's. Thus, the mass of the  $D^0$  candidates was required to lie between 1.55 and 1.70 GeV/c<sup>2</sup>. The value of  $\cos \theta^*$  was required to be greater than  $-0.8$ . The dE/dx measurement in the TPC and the kaon identification in the RICH detector were used to validate the kaon assignment for the  $D^0$  candidate. If no particle identification was available, the particle was kept as a kaon candidate. The distribution of the mass difference  $\Delta M$  obtained by applying the above selection criteria is shown in Fig. 1b. In the range of  $\Delta M$  between 0.140 and 0.152 GeV/c<sup>2</sup>, 3610 events are observed; about 55% are expected to be true  $D^{*\pm}$ .

- $D^0 \rightarrow K^- \pi^+ \pi^+ \pi^-$ .

The invariant mass  $M(K^- \pi^+ \pi^- \pi^+)$  was required to be between 1.84 and 1.88 GeV/c<sup>2</sup>. A fit to a common vertex was performed with the five tracks from the  $D^{*\pm}$  decay, and the invariant mass of the combination  $M(K^- \pi^+ \pi^- \pi^+ \pi^+)$  was restricted to the interval (1.975-2.050) GeV/c<sup>2</sup>. To reduce the combinatorial back-



ground, particle identification information was used for the candidate kaon from the  $D^0$ . The assignment was rejected if the kaon hypothesis was vetoed by the RICH detector, or if the measured  $dE/dx$  was consistent with the pion mass hypothesis and inconsistent with the kaon one. To reduce the level of combinatorial background further, a requirement on the  $\chi^2$ -probability of the  $D^{*\pm}$  vertex fit was applied. The loss induced by this requirement was checked using the subsample of  $D^{*\pm}$  with  $X_{D^*}$  between 0.35 and 0.5. These events were divided into two categories, above and below the  $\chi^2$ -probability cut. The spectrum of the mass difference  $\Delta M = M(K^-\pi^+\pi^-\pi^+) - M(K^-\pi^+\pi^-\pi^+)$  shows a clear  $D^{*\pm}$  peak for the above-cut category, and no significant signal is observed in the other. The  $\Delta M$  distribution obtained is shown in Fig. 1c. In the range  $0.144 < \Delta M < 0.147$  GeV/ $c^2$ , 7655 events are observed, and 25% of which are expected to be true  $D^{*\pm}$ .

## 5.2 Decay length reconstruction

The determination of the decay length  $d$  relies on the reconstruction of primary and secondary vertices. The mean positions of the beam in the horizontal ( $x$ ) and vertical directions ( $y$ ) was measured from the data, for every 100 hadronic  $Z^0$  decays, with an accuracy close to 10  $\mu\text{m}$  in  $x$  and  $y$ . The event main vertex was obtained by using all the reconstructed charged particle trajectories in the event and finding a common intersection point, compatible with the beam profile ( $\sigma_x = 150$   $\mu\text{m}$ ,  $\sigma_y = 10$   $\mu\text{m}$ , but here the effective vertical size of the beam interaction region is enlarged to 40  $\mu\text{m}$  to allow for possible misalignments). Tracks giving the largest contribution to the  $\chi^2$  were successively eliminated until an acceptable vertex fit probability was obtained. For a  $b\bar{b}$  event, the accuracy of the primary vertex reconstruction is 68  $\mu\text{m}$  in  $x$  and 35  $\mu\text{m}$  in  $y$ .

The  $D^0$  decay point was reconstructed from the  $K^-\pi^+\pi^+(\pi^0)$  and  $K^-\pi^+\pi^-\pi^+$  combinations. The distance from the primary vertex to the  $D^0$  decay vertex was first calculated in the plane transverse to the beam axis. The value of this distance was attributed a negative or positive sign in accordance with the sign of the scalar product of the momentum vector of the  $D^{*\pm}$  and of the vector joining the primary to the secondary vertex. The decay length  $d$  was then determined in space by using the  $D^{*\pm}$  meson direction. The average precision on the decay length was found to be  $\sigma_d \simeq 300$   $\mu\text{m}$  from a simulation study. Events with a decay length in the range  $-0.5$  cm  $< d < 3.0$  cm were accepted.

## 5.3 Probability distributions and fitting procedure

The time distributions corresponding to the secondary  $D^0$  vertices were obtained for each of the expected components of the  $D^{*\pm}$  candidates by convoluting the theoretical proper time distribution with Gaussian functions to account for the experimental accuracy in the proper time.

The  $B_d^0$  proper time,  $t_B = m_B d_B / p_B$ , where  $m_B$ ,  $d_B$ , and  $p_B$  are the  $B_d^0$  mass, decay distance, and momentum respectively, was not measured directly, since only the  $D^*$  decay products were reconstructed. The measured decay distance was the sum of the  $B_d^0$  and  $D^0$  decay distances,  $d \simeq d_B + d_D$ . To take into account the  $D^0$  decay distance, a new variable was defined for each event, which was the sum of the  $B_d^0$  and  $D^0$  proper times,  $t = t_B + t_D$ . The theoretical probability distributions for the variable  $t$  were obtained by convoluting the time dependent probability distributions (2) and (3) with the exponential  $D^0$  decay distribution  $\frac{1}{\tau_D} e^{-t_D/\tau_D}$ , where  $\tau_D$  is the  $D^0$  lifetime.

The sum of  $B_d^0$  and  $D^0$  proper times can be written as:

$$t = t_B + t_D = \frac{m_B}{p_B} d_B + \frac{m_D}{p_D} d_D = \frac{m_B}{p_B} d + \left( \frac{m_D}{p_D} - \frac{m_B}{p_B} \right) d_D \simeq \frac{m_B}{p_B} d, \quad (9)$$

where the term proportional to  $d_D$  was neglected, being of order of a percent with respect to the other. The  $B_d^0$  momentum in equation (9) was taken as the mean fraction of the beam momentum carried by the  $B_d^0$ . It was verified with the Monte Carlo simulation that the average fraction of the beam energy taken by the  $B_d^0$  is slightly affected by the  $D^{*\pm}$  selection criteria, and a correction was applied accordingly. Parametrizing the  $B_d^0$  momentum as a function of the reconstructed  $D^{*\pm}$  momentum was also studied. The resolution on  $t$  improved slightly by using such a parametrization, but the effect on the measurement of  $\Delta m_d$  was negligible. Therefore, the simpler approximation of the average  $B_d^0$  momentum,  $p_B \simeq 0.7 p_{beam}$ , was used. The validity of the approximations involved in equation (9) was verified on a set of generated  $B_d^0$  events, passed through a detailed simulation of the detector. The average resolution on  $t$  was found to be 0.4 ps, which is sufficient for the measurement of the time dependent  $B_d^0$  mixing. The final normalized probability distributions  $\mathcal{P}_{B^0}^{mix(unmix)}(t, \Delta m_d)$  were obtained by convoluting the theoretical probabilities for the variable  $t$  with a Gaussian resolution function of standard deviation  $\sigma_t = \left[ (\sigma_d/d)^2 + (\sigma_{p_{B^0}}/p_{B^0})^2 \right]^{\frac{1}{2}} t$ , where  $\sigma_d$  was evaluated event by event (the typical value was given in Sect. 5.2). An average value for  $\sigma_{p_{B^0}}/p_{B^0} = 0.17$  was used, as determined from the simulation. The choice of a Gaussian distribution for  $p_{B^0}$  did not properly describe the resolution of the  $B_d^0$  momentum, but this approximation was adequate for the present measurement.

For charged B mesons, the normalized probability distribution  $\mathcal{P}_{B^\pm}(t)$  was determined in a similar way as for  $\mathcal{P}_{B^0}^{mix(unmix)}(t, \Delta m_d)$ , but without including the oscillation terms of expressions (2) and (3).

When the  $D^{*\pm}$  originates from a  $c\bar{c}$  event, the variable  $t$  defined previously differs from the  $D^0$  proper time by the ratio between the real  $D^0$  and the supposed  $B_d^0$  boosts. The corresponding time distribution  $\mathcal{P}_C(t)$  was determined from the Monte Carlo simulation and parametrized with an exponential distribution.

The time distribution corresponding to the events from the combinatorial background under the  $D^{*\pm}$  peak,  $\mathcal{P}_{comb}(t)$ , was obtained from the upper sideband of the  $\Delta M$  mass distribution, by requiring  $\Delta M > 0.15, 0.15 (0.16)$  GeV/ $c^2$  for the  $K\pi, K\pi\pi\pi (K\pi\pi^0)$  candidates. The possibility of a time dependent oscillating contribution from the combinatorial background was studied by comparing the ratio of the time distributions of unlike to like-sign events. No evidence for such a contribution was found, and the same distribution  $\mathcal{P}_{comb}(t)$  was used for like and unlike-sign events.

The maximum likelihood method was used to fit the time distributions for the unlike and like-sign events. The probability density function used to construct the likelihood function for unlike-sign events was written as:

$$\begin{aligned} \mathcal{L}^{unlike} &= f_{B^0} \left[ \epsilon_b^{D^*} \mathcal{P}_{B^0}^{mix}(t, \Delta m_d) + (1 - \epsilon_b^{D^*}) \mathcal{P}_{B^0}^{unmix}(t, \Delta m_d) \right] \\ &+ f_{B^\pm} \epsilon_{B^\pm}^{unlike} \mathcal{P}_{B^\pm}(t) \\ &+ f_{c\bar{c}} \epsilon_{c\bar{c}}^{unlike} \mathcal{P}_C(t) \\ &+ f_{comb} \epsilon_{comb}^{unlike} \mathcal{P}_{comb}(t), \end{aligned} \quad (10)$$

where

- $f_{B^0}, f_{B^\pm}, f_{c\bar{c}}$ , and  $f_{comb}$  are the fractions of  $B_d^0, B^\pm, c\bar{c}$ , and of the combinatorial background in the selected sample of events;

- $\epsilon_b^{D^*}$  is the probability of correctly identifying the  $b$  or  $\bar{b}$  quark in the hemisphere opposite to the  $D^{*\pm}$  and includes also the fact that there are  $\overline{B^0} \rightarrow D^{*-} X$  where the correlation between the B flavour and the  $D^{*\pm}$  charge is opposite to the one of standard decays;
- $\epsilon_{B^\pm, c\bar{c}, comb}^{unlike}$  are the probabilities of tagging  $B^\pm$ ,  $c\bar{c}$ , and combinatorial background events as unlike-sign candidates.
- From the simulation, the contribution from  $B_s^0$  mesons was found to be negligible and is therefore not considered.

The likelihood function for like-sign events  $\mathcal{L}^{like}$  was obtained by substituting all the purities  $\epsilon$  in (10) by  $(1 - \epsilon)$ . The values used for the different parameters in (10) are given in Sect. 5.4.

## 5.4 Experimental results and consistency checks

The amplitude of the time dependent oscillation is sensitive to the probability of correctly tagging events as unmixed and mixed  $B_d^0$ . Therefore, only events having  $|Q_{hem}| > 0.1$  (see Sect. 4) were used. In order to be insensitive to details of the Monte Carlo simulation, the maximum likelihood fit was performed leaving free both  $\Delta m_d$  and the probability  $\epsilon_b^{D^*}$  (defined in Sect. 5.3). Both  $\tau_B$  and  $\tau_D$  were fixed to the current world averages. The values of  $\epsilon_{B^\pm}^{unlike}$ ,  $\epsilon_{c\bar{c}}^{unlike}$ , and  $f_{B^\pm}$  were taken from the simulation, as was the effective time distribution of charm events. The remaining parameters and time distributions were determined from the data. The values obtained for  $f_{comb}$ ,  $\epsilon_{comb}^{unlike}$ , and  $r_{c\bar{c}}$  are summarised in Tab. 2. They were obtained as follows.

- The combinatorial background fractions,  $f_{comb}$ , were obtained from fits to the  $\Delta M$  spectra. The signals were parametrized with two Gaussian distributions ( $K\pi$ ,  $K\pi\pi^0$ ) and a Breit-Wigner distribution ( $K\pi\pi\pi$ ), and the backgrounds with polynomials.
- The fractions  $\epsilon_{comb}^{unlike}$  of unlike-sign events in the combinatorial background were determined by using the events outside the  $D^{*\pm}$  peaks in the  $\Delta M$  spectra.
- The fraction  $r_{c\bar{c}}$  of  $D^{*\pm}$  originating from charm quark fragmentation,  $r_{c\bar{c}} = f_{c\bar{c}} / (f_{c\bar{c}} + f_{B^0} + f_{B^\pm})$ , was obtained by fitting the measured  $X_{D^*}$  distributions to the sum of the distributions expected for  $b\bar{b}$  and  $c\bar{c}$  events, taken from the simulation. The values obtained were in agreement with those obtained from the simulation.

The  $B_d^0$  momentum was fixed according to the measured average fraction of the beam energy carried by B hadrons given in Tab. 1. This value was increased by 6%, according to the bias observed in simulated events due to the  $D^{*\pm}$  selection criteria.

Using these parameters, the result of the combined fit to the samples of  $K\pi$ ,  $K\pi\pi^0$  and  $K\pi\pi\pi$  candidates was:

$$\Delta m_d = 0.523 \pm 0.072 \text{ ps}^{-1}, \quad \epsilon_b^{D^*} = 0.65 \pm 0.02. \quad (11)$$

The fitted value of  $\epsilon_b^{D^*}$  may be compared with the measured value of  $\epsilon_b^Q = 0.673 \pm 0.005$  obtained with the independent measurement described below in Sect. 6.3.2. However, it should be noticed that  $\epsilon_b^{D^*}$  and  $\epsilon_b^Q$  are not expected to be exactly equal, because there are suppressed decays  $\overline{B^0} \rightarrow D^{*-} X$ , where the correlation between the B flavour and the  $D^{*\pm}$  charge is opposite to that in standard decays. These processes therefore tend to reduce the value of  $\epsilon_b^{D^*}$  with respect to  $\epsilon_b^Q$ .

The experimental distributions of the decay distance for unlike and like-sign events are shown in Fig. 2, with the result of the fit superimposed. The experimental distribution

of the fraction of unlike-sign events versus the decay distance is shown in Fig. 3, with the result of the fit superimposed.

Several systematic checks were performed:

- Fitting the B lifetime after fixing the charm and background time distributions and fractions previously determined yielded  $\tau_B = 1.58 \pm 0.06$  ps, in agreement with the world average [12].
- An estimate of  $\epsilon_{c\bar{c}}^{unlike}$  was obtained from the data in the following way. Events rejected by the requirement  $X_{D^*} > 0.50$  are enriched in  $c\bar{c}$  events ( $\simeq 80\%$ ). The number of unlike-sign events in this sample, using the charge correlation efficiencies for non-charm events found in the simulation, gave  $\epsilon_{c\bar{c}}^{unlike} = 0.67 \pm 0.02$ , in agreement with the value  $0.65 \pm 0.01$  found in the simulation.
- Leaving the fractions of  $c\bar{c}$  events free in the fit yielded  $r_{c\bar{c}}^{K\pi, K\pi\pi\pi} = 0.387 \pm 0.025$  and  $r_{c\bar{c}}^{K\pi\pi^0} = 0.41 \pm 0.03$ , in agreement with the measured values given in Tab. 2.
- The effect of a possible bias induced by the vertex  $\chi^2$ -probability cut in the  $D^0 \rightarrow K^-\pi^+\pi^+\pi^-$  channel was studied. Using a simulated sample of pure  $B_d^0$  mesons,  $\Delta m_d$  was determined with and without the probability cut, and no significant differences were observed.
- The fit was repeated using a parametrization of the  $B_d^0$  momentum as a function of the reconstructed  $D^{*\pm}$  momentum. The fitted value of  $\Delta m_d$  changed by only 1% from the value obtained assuming the  $B_d^0$  carried a fixed fraction of the beam energy.
- Applying the fitting procedure to a fully simulated event sample generated with  $\Delta m_d = 0.475$  ps $^{-1}$  yielded  $\Delta m_d = 0.48 \pm 0.06$  ps $^{-1}$ .

## 5.5 Systematic uncertainties

Various possible sources of systematic uncertainties were investigated. In the following, the systematic errors on  $\Delta m_d$  were estimated by varying the relevant parameters by one standard deviation. The results are summarised in Tab. 3. The sign ( $\pm$  or  $\mp$ ) of the error assigned to  $\Delta m_d$  shows the correlation with the variation of the relevant parameters.

- *Time parametrization and B momentum resolution.*  
Different parametrizations for the time distributions of charm and combinatorial background events were used. The parametrizations for the combinatorial background distribution were varied according to the limited data statistics used for its determination. The observed variations on  $\Delta m_d$  were negligible. Varying the  $B_d^0$  decay length resolution by  $\pm 20\%$  changed  $\Delta m_d$  by  $\pm 0.002$  ps $^{-1}$ . Changing the B momentum resolution  $\sigma_{p_{B^0}}/p_{B^0} = 0.17 \pm 0.03$  by its uncertainty changed the fitted value of  $\Delta m_d$  by  $\pm 0.020$  ps $^{-1}$ .
- *B and D lifetimes.*  
The values of the B and D lifetimes were varied according to their experimental errors [12]. Changes in  $\Delta m_d$  of  $\mp 0.004$  ps $^{-1}$  and  $\pm 0.001$  ps $^{-1}$ , respectively, were observed.
- *B momentum parametrization.*  
According to the simulation, the mean fraction of the beam energy taken by the B meson increases by  $(6 \pm 1)\%$  after the  $D^{*\pm}$  selection. The corresponding uncertainty was added in quadrature to the error on  $\langle X_E \rangle$  [16] in order to estimate the corresponding systematic uncertainty on  $\Delta m_d$  of  $\mp 0.007$  ps $^{-1}$ .
- *Fractions  $r_{c\bar{c}}$ ,  $f_{comb}$  and  $f_{B^\pm}$ .*  
The fractions  $r_{c\bar{c}}$  and  $f_{comb}$  were varied according to the values reported in Tab. 2.

Both  $r_{c\bar{c}}$  and  $f_{comb}$  contributed  $\pm 0.003 \text{ ps}^{-1}$  to the systematic error. The relative importance of neutral and charged B decays in the selected  $D^{*\pm}$  sample, which determines the fractions  $f_{B^0}$  and  $f_{B^\pm}$ , was taken from the  $D^{*\pm}$  production rate in the semileptonic decays. As shown below in Sect. 6.4.2, the process  $\overline{B}_d^0 \rightarrow D^{*+} \ell^- \overline{\nu}_\ell X$  accounts for  $(83.2 \pm 4.1)\%$  of the  $D^{*\pm}$  production in semileptonic decays. Assuming factorization, this evaluation can also be used for inclusive  $D^{*\pm}$  production. A ratio  $\frac{N_{B^\pm}}{N_{B^0} + N_{B^\pm}} = 0.17$  was used with a conservative uncertainty of  $\pm 50\%$  related to the assumption of factorization, giving a systematic uncertainty on  $\Delta m_d$  of  $\pm 0.035 \text{ ps}^{-1}$ .

- *Hemisphere charge probabilities.*

The hemisphere charge probabilities  $\epsilon_{comb}^{unlike}$  were varied according to Tab. 2, giving a change of  $\mp 0.005 \text{ ps}^{-1}$  on  $\Delta m_d$ . For the probability  $\epsilon_{c\bar{c}}^{unlike}$ , the value  $0.67 \pm 0.02$  was measured on the data (see Sect. 5.4). The corresponding uncertainty on  $\Delta m_d$  was  $\pm 0.005 \text{ ps}^{-1}$ . The hemisphere charge probability  $\epsilon_{B^\pm}^{unlike}$  was varied according to the Monte Carlo value  $0.33 \pm 0.03$ , where the large error is due to a lack of knowledge concerning the suppressed decays  $B^\mp \rightarrow D^{*\pm} X$  with an opposite correlation between the charges of the B and D mesons. The effect on  $\Delta m_d$  was  $\mp 0.011 \text{ ps}^{-1}$ .

The total systematic error on  $\Delta m_d$  deduced was  $\pm 0.043 \text{ ps}^{-1}$ . Thus the mass difference between the two physical  $B_d^0$  states measured in the  $D^{*\pm} - Q_{hem}$  channel is

$$\Delta m_d = 0.523 \pm 0.072 \pm 0.043 \text{ ps}^{-1}. \quad (12)$$

## 6 Measurements of $\Delta m_d$ in inclusive channels

In all these three analyses, described in Sects. 6.3 to 6.5, the decay sign was determined by a high  $p_t$  lepton. Events with an identified lepton with a transverse momentum  $p_t$  larger than  $1.2 \text{ GeV}/c$  relative to its jet axis were selected. The lepton was removed from the jet before evaluating its transverse momentum. Sects. 6.1 and 6.2 describe methods used in the three analyses.

### 6.1 Inclusive B hadron reconstruction

The semileptonic B hadron decays were reconstructed using the track classification provided by a general algorithm developed to reconstruct the decay vertex of the B hadron.

The event main vertex was determined following the procedure explained in Sect. 5.2.

The B secondary vertex was obtained by intersecting the trajectories of the lepton and of a D candidate. The lepton track and at least one of the charged particles assigned as a D decay product had to be associated to hits in the VD. Particles from fragmentation and from B decay products are all present in the jet which contains the lepton, so an approach was developed to distinguish between them. Ignoring the lepton, charged particles belonging to the jet were gathered into low mass clusters, using LUCLUS with the parameter  $d_{join}$  reduced to  $0.5 \text{ GeV}$  and assuming the particles to be pions. Inside each cluster, the particles were ordered by decreasing values of their pseudo-rapidity relative to the cluster direction. Those having the largest pseudo-rapidity values and a momentum larger than  $500 \text{ MeV}/c$  were then kept until the mass of the resulting system exceeded  $2.2 \text{ GeV}/c^2$ . Clusters which made an angle larger than  $500 \text{ mrad}$  relative to the jet direction were discarded. If a cluster contained more than one particle measured in the VD, a secondary vertex was obtained from the particles belonging to the cluster, a pseudo-D

track candidate was constructed, and the intersection of the pseudo-D track with the lepton trajectory was evaluated. If a cluster contained only one particle measured in the VD, its intersection with the lepton trajectory was evaluated. Among all these secondary vertices, the one which has the largest statistical significance<sup>‡</sup> was kept.

Having selected the cluster which had the best chance to contain a majority of D decay products, and to reduce possible biases on the measured decay length of the B hadron induced by this selection, this cluster was used simply as a seed to find the other particles emitted by the D, which might be in other clusters. For this purpose, all particles present in the jet, including neutrals but not the lepton, were ordered by decreasing values of their pseudo-rapidity relative to the direction of the momentum sum of the previously retained particles. Then particles were added to the previously retained ones until the mass of the system exceeded  $2.2 \text{ GeV}/c^2$ . A new evaluation of the D candidate trajectory was then obtained, and a secondary vertex was constructed with the lepton track. All of the retained particles were then called B decay products.

## 6.2 Measurement of the B decay proper time

The B decay proper time was measured from the estimates of the B decay distance and momentum:

$$t_B = \frac{d_B m_B}{p_B} \quad (13)$$

### 6.2.1 B decay distance

The B decay distance  $d_B$  was obtained from the projected distance  $d_P$  between the secondary and the primary vertices measured in the  $xy$  plane, from which  $d_B$  is then evaluated along the jet direction in space:  $d_B = d_P/\sin \theta$ .

The accuracy on the measurement of the positions of charged particles near the beam interaction region, given by the simulation, was tuned to agree with the accuracy observed in the real data. For this purpose, tracks emitted at an angle less than  $30^\circ$  from the horizontal plane were selected, so as to benefit from the precise definition of the beam position in the vertical direction. The tuning procedure is as follows [17].

Firstly, the measurement errors on the  $R\Phi$  and  $z$  impact parameters in the simulation are rescaled to agree with those from real data for tracks associated to the same numbers of VD hits and with a similar momentum.

A lifetime-signed impact parameter, relative to the event main vertex, is positive if the track intercepts the line defined by the main vertex and the jet direction at a positive distance from the vertex in the direction of the jet momentum. Negative values then arise primarily from measurement errors. Therefore, distributions of negative lifetime-signed impact parameters, divided by their errors, are compared between data and simulation. They are fitted with a Gaussian and two Breit-Wigner functions centred on zero.

The narrowest distribution is the Gaussian. It contains the largest fraction of events and its standard deviation, measured on data, is always larger than unity. A scaling factor is then applied to the impact parameter errors so that the width of the distribution becomes unity for the real data. The same scaling is applied in the simulation, and an additional smearing of the values of the simulated impact parameters is usually needed to have normal distributions with unit variance also here. The fractions of events present in the Breit-Wigner distributions and the widths of these distributions are usually larger

---

<sup>‡</sup>The statistical significance is defined as the distance between the secondary and the primary vertices along the jet direction, evaluated in the plane transverse to the beam axis, divided by its measurement error.

for real data. A further smearing of the simulated impact parameters is then applied so as to obtain a behaviour similar to that in data for the non-Gaussian tails.

The vertex algorithm described in Sect. 6.1 provides a measurement of the B decay distance in 94% of the events containing a high  $p_t$  lepton associated to at least one hit in the VD. The remaining 6% of the events were rejected.

### 6.2.2 B momentum

The B momentum was determined in several steps. First, each event was divided into two hemispheres separated by the plane transverse to the sphericity axis which contains the beam interaction region. Then the momentum of the B meson,  $P_{meas.}^B$ , was evaluated from the energy-momentum of the hemisphere after subtracting the particles not selected as B decay products (see Sect. 6.1). Then, to have a better estimate of the B momentum, the measured energies and momenta were rescaled by a common factor ( $\alpha$ ) and a missing four-momentum corresponding to a zero mass particle was added ( $E_\nu, \vec{P}_\nu$ ). After having applied the energy and momentum conservation to the complete event,

$$\alpha \times (\vec{P}_{hem1} + \vec{P}_{hem2}) + \vec{P}_\nu = \vec{0} \quad (14)$$

$$\alpha \times (E_{hem1} + E_{hem2}) + E_\nu = 2 E_{beam} \quad (15)$$

the unknowns were determined. The mean value of  $\alpha$  was 1.13. If the direction of the missing momentum was within 400 mrad of that of the D- $\ell$  system, its energy was attributed to the B to account for the missing neutrino. A better approximation to the B momentum was then obtained using the simulation, by correcting for the average difference between the above estimator and the true B momentum, parametrized as a function of the reconstructed B momentum.

Finally a global fit was applied to all the measured quantities: the primary and secondary vertex positions (6 variables), and the momentum vectors of the lepton and of the D and B mesons (9 variables). Three constraints were applied:

- the direction given by the two vertices and the direction of the B momentum should be the same (two angular constraints),
- the mass of the B meson should be equal to the nominal  $B_d^0$  mass.

### 6.2.3 Proper time resolution

The reconstruction accuracy on the positions of the charged particles near the beam interaction region was verified on real data by selecting event samples depleted in B meson decays [17]. To have a detailed description of the time resolution, the distribution of the difference between the generated ( $t'$ ) and reconstructed ( $t$ ) B decay proper times  $\mathcal{R}_B(t' - t)$  was parametrized using the sum of a Gaussian and a Breit-Wigner distribution with widths that depended on the generated decay time and which were different depending on the sign of  $t' - t$ .

For about 10% of the events, because of the presence of charged particles coming from the beam interaction region, the reconstructed vertex coincided with the event main vertex. A Breit-Wigner distribution, centred on  $t = 0$ , was used to account for the proper time distribution of these events.

The accuracy on the B decay proper time is degraded in the case of cascade semileptonic decays <sup>§</sup>, since the parametrization of the difference between the true and measured

<sup>§</sup>In this paper *cascade decays* refers to the decay  $b \rightarrow c \rightarrow \text{lepton}$

B momentum and the strategy for reconstructing the B decay point were tuned assuming a direct semileptonic decay of a B hadron. This effect was verified using the simulation, and a different parametrization,  $\mathcal{R}_{BC}(t' - t)$ , was extracted for this category of leptons.

Finally the simulated time distribution for accepted events was compared with an exponential distribution corresponding to the generated lifetime and an acceptance function,  $\mathcal{A}(t')$ , was obtained.

Sets of parametrizations were obtained separately for the 1991 to 1993 and for 1994 data sample, because of the installation of the double sided silicon vertex detector at the end of 1993.

For events originating from light and charm quark flavours, the expected time distributions,  $\mathcal{P}_H(t)$  and  $\mathcal{P}_C(t)$ , were obtained from the simulation.

## 6.3 The lepton- $Q_{hem}$ channel

In this analysis method, the decay sign is obtained from the lepton charge and the production sign is measured using the hemisphere charge in the opposite hemisphere, as in the exclusively reconstructed  $D^*$  analysis.

### 6.3.1 Composition of the lepton sample

Muons were identified by combining the muon chamber hits with the tracking information. The tracks of charged particles were extrapolated to the muon chambers and then associated and fitted to the hits. The muon identification algorithm is described in [7]. The loose selection criterion had an efficiency of 95 %, within the acceptance of the muon chambers, with a misidentification probability of 1.5 %. Tighter cuts gave 76 % efficiency with 0.44 % misidentification probability.

The electron candidates were identified by combining the electromagnetic shower information from the HPC with the particle ionization loss,  $dE/dx$ , measured by the TPC. A sizeable fraction of electrons originates from photon conversions. They were partially rejected if two oppositely charged particles form a secondary vertex where the invariant mass was zero within measurement errors. Inside the acceptance of the HPC, electrons of momenta above 3 GeV/c were identified with an efficiency of 77 %. The probability for a hadron to be misidentified as an electron was below 1 %.

The efficiency to identify leptons and the hadronic contamination were obtained using the detailed simulation code of the DELPHI detector, and were checked on the data using selected event samples such as  $K_s^0 \rightarrow \pi^+\pi^-$ ,  $Z^0 \rightarrow \mu^+\mu^-$ , converted photons before the HPC,  $\gamma\gamma \rightarrow \ell^+\ell^-$ , and hadronic  $\tau$  decays [7].

Candidate leptons were produced by semileptonic decays of B hadrons, D hadrons, and light mesons. They also could be misidentified hadrons or converted photons. Leptons from cascade decays have wrong sign with respect to leptons from direct B decays for the identification of the  $b$  quark charge. Therefore, cuts were applied to the lepton total and transverse momenta to minimize their contribution. The cut values were determined by maximizing the product  $(f_b^\ell - f_{bc}^\ell) \times \sqrt{N_\ell}$ , where  $f_b^\ell$  and  $f_{bc}^\ell$  are the respective fractions of direct and cascade leptons in the total sample of  $N_\ell$  lepton candidates. The fractions of the different categories of selected leptons, with  $p_t > 1.2$  GeV/c and momentum  $p$  larger than 3 GeV/c, were obtained from the simulation and were also measured in the data by fitting the  $(p, p_t)$  distributions of the different components to the corresponding distribution for lepton candidates observed in the data.



To study  $B$ - $\bar{B}$  oscillations, lepton candidates in the simulated event sample were distributed into four classes according to their sign relative to the sign of the heavy quark present in the decaying hadron.

- Class  $\ell_b$  contained lepton candidates produced in  $B$  hadron decays and having the same sign as the  $b$  quark present inside the  $B$  hadron. This class contained leptons from direct  $b$  semileptonic decays and also, for example, those from cascade decays of the type:  $\bar{B} \rightarrow D\bar{D}_s X$  with  $\bar{D}_s \rightarrow \ell^- X$ . Misidentified hadrons with the same sign as the  $b$  quark were also included if they originated from a track produced in a  $B$  hadron decay.
- Class  $\ell_{bc}$  contained lepton candidates produced in  $B$  hadron decays and having a sign opposite to the  $b$  quark.
- Class  $\ell_c$  contained lepton candidates produced in charmed hadron decays.
- Class  $\ell_h$  contained lepton candidates which were misidentified hadrons or leptons produced in light hadron decays or were from converted photons and which had not fallen into the previous classes.

With these definitions, if a  $B$  hadron oscillated, lepton candidates in classes  $\ell_b$  and  $\ell_{bc}$  changed sign, whereas those in the other classes were not affected.

The semileptonic decay branching fractions used in the simulation were modified to agree with the measured values quoted in Tab. 1.

The fraction of fake lepton candidates was verified in the data with an accuracy of  $\pm 20\%$  on the basis of time distributions.

After having corrected the simulation so that the rates of the physics processes and their simulation agreed with the data, the fractions of lepton candidates in the different classes were:

$$f_b^\ell = 70.2\%, \quad f_{bc}^\ell = 7.5\%, \quad f_c^\ell = 9.4\%, \quad f_h^\ell = 12.9\% \quad (1991 - 1993) \quad (16)$$

and

$$f_b^\ell = 71.9\%, \quad f_{bc}^\ell = 8.1\%, \quad f_c^\ell = 9.4\%, \quad f_h^\ell = 10.6\% \quad (1994) \quad (17)$$

for candidates of momentum larger than 3 GeV/c and transverse momentum larger than 1.2 GeV/c. Uncertainties attached to these fractions depend on the semileptonic branching fraction measurements, on the lepton identification procedure, and on the rate of the fake lepton background. They are discussed in Sect. 6.3.3.

The measurement of  $B$  meson oscillations is not critical with respect to the selection on the lepton transverse momentum in the range between 0.8 and 1.4 GeV/c.

### 6.3.2 Measurement of $\Delta m_d$

Events were classified on the basis of the product of the charge of the lepton,  $Q_\ell$ , identified in one hemisphere, and of the mean charge,  $Q_{hem}$ , measured in the opposite hemisphere. Events were considered as mixed if  $Q_{hem} \times Q_\ell > 0.1$ , and as unmixed if  $Q_{hem} \times Q_\ell < -0.1$ . The numbers of events in the mixed and unmixed categories were 24051 and 36330 respectively.

For each event, the probability to obtain the measured proper time  $t$ ,  $\mathcal{P}^{like}(t)$  or  $\mathcal{P}^{unlike}(t)$  depending on its classification, was evaluated:

$$\begin{aligned}
\mathcal{P}^{like}(t) &= f_b \sum_q F_{B_q} [\epsilon_b^Q \epsilon_{B_q}^\ell (\mathcal{P}_{B_q}^{mix.}(t') \otimes \mathcal{R}_B(t' - t)) \\
&\quad + (1 - \epsilon_b^Q)(1 - \epsilon_{B_q}^\ell) (\mathcal{P}_{B_q}^{mix.}(t') \otimes \mathcal{R}_{BC}(t' - t)) \\
&\quad + (1 - \epsilon_b^Q) \epsilon_{B_q}^\ell (\mathcal{P}_{B_q}^{unmix.}(t') \otimes \mathcal{R}_B(t' - t)) \\
&\quad + \epsilon_b^Q (1 - \epsilon_{B_q}^\ell) (\mathcal{P}_{B_q}^{unmix.}(t') \otimes \mathcal{R}_{BC}(t' - t))] \\
&\quad + f_c \epsilon_c^{like} \mathcal{P}_C(t) \\
&\quad + f_h \epsilon_h^{like} \mathcal{P}_H(t)
\end{aligned} \tag{18}$$

$$\begin{aligned}
\mathcal{P}^{unlike}(t) &= f_b \sum_q F_{B_q} [\epsilon_b^Q \epsilon_{B_q}^\ell (\mathcal{P}_{B_q}^{unmix.}(t') \otimes \mathcal{R}_B(t' - t)) \\
&\quad + (1 - \epsilon_b^Q)(1 - \epsilon_{B_q}^\ell) (\mathcal{P}_{B_q}^{unmix.}(t') \otimes \mathcal{R}_{BC}(t' - t)) \\
&\quad + (1 - \epsilon_b^Q) \epsilon_{B_q}^\ell (\mathcal{P}_{B_q}^{mix.}(t') \otimes \mathcal{R}_B(t' - t)) \\
&\quad + \epsilon_b^Q (1 - \epsilon_{B_q}^\ell) (\mathcal{P}_{B_q}^{mix.}(t') \otimes \mathcal{R}_{BC}(t' - t))] \\
&\quad + f_c (1 - \epsilon_c^{like}) \mathcal{P}_C(t) \\
&\quad + f_h (1 - \epsilon_h^{like}) \mathcal{P}_H(t)
\end{aligned} \tag{19}$$

where

- $f_b$ ,  $f_c$  and  $f_h$ , which satisfy  $f_b + f_c + f_h = 1$ , are the respective fractions of  $b$ ,  $c$ , and  $u, d, s$  flavours in the analyzed event sample (see Sect. 6.3.1.),

$$f_b = f_b^\ell + f_{bc}^\ell, \quad f_c = f_c^\ell, \quad f_h = f_h^\ell; \tag{20}$$

- $F_{B_q}$  is the fraction of B hadrons of flavour  $q$  in the sample;
- $\epsilon_b^Q$  and  $\epsilon_{B_q}^\ell$  are the probabilities to have the right sign for the quark at production and decay times, respectively;  $\epsilon_b^Q$  is the purity of the tagging given by the hemisphere charge, measured in the hemisphere opposite to the lepton, and its value was fitted to the data simultaneously with  $\Delta m_d$ ;
- in  $Z^0 \rightarrow c\bar{c}$  events and for light flavours,  $\epsilon_c^{like}$  and  $\epsilon_h^{like}$  are the fractions of events classified as mixed candidates from the relative signs of the lepton and the hemisphere charge; their values were obtained from the simulation:

$$\epsilon_c^{like} = 0.370 \pm 0.005, \quad \epsilon_h^{like} = 0.451 \pm 0.005; \tag{21}$$

- $\mathcal{P}_{B_q}^{mix.}(t') \otimes \mathcal{R}_B(t' - t) = \int \mathcal{P}_{B_q}^{mix.}(t') \mathcal{R}_B(t' - t) dt'$  and similarly for the analogous terms. The variable  $t'$  is the true proper time of the B decay. For neutral B mesons, the functions  $\mathcal{P}_{B_q}^{mix.}(t')$  and  $\mathcal{P}_{B_q}^{unmix.}(t')$  were given in Sect. 1. For charged B mesons and  $b$  baryons, the decay time distribution has a simple exponential behaviour. These distributions have to be convoluted with the time resolution distributions,  $\mathcal{R}_B(t' - t)$  and  $\mathcal{R}_{BC}(t' - t)$  for direct and cascade semileptonic B decays respectively, obtained from the simulation.
- For  $Z^0 \rightarrow c\bar{c}$  and  $Z^0 \rightarrow (light\ flavour)$  events, the reconstructed time distributions obtained in the simulation were fitted directly to provide  $\mathcal{P}_C(t)$  and  $\mathcal{P}_H(t)$ .

A maximum likelihood method was applied to the set of classified events, and the parameters  $\Delta m_d$  and  $\epsilon_b^Q$  were fitted by minimizing the following function :

$$\mathcal{L} = - \sum_{like\text{-}sign\text{ events}} \ln(\mathcal{P}^{like}(t)) - \sum_{unlike\text{-}sign\text{ events}} \ln(\mathcal{P}^{unlike}(t)). \tag{22}$$

The result of the fit is:

$$\Delta m_d = 0.493 \pm 0.042 \text{ ps}^{-1}, \quad \epsilon_b^Q = 0.673 \pm 0.005. \quad (23)$$

The experimental decay time distributions for like and unlike-sign events are shown in Fig. 4, with the result of the fit superimposed. The experimental distribution of the fraction of like-sign events versus the decay time is shown in Fig. 5.

The internal coherence of the fitting procedure was verified using a fast simulation with 60 times the data statistics. The result :

$$\Delta m_d = 0.453 \pm 0.004 \text{ ps}^{-1} \quad (\text{fast simulation}) \quad (24)$$

is in agreement with the generated value of  $\Delta m_d = 0.45 \text{ ps}^{-1}$ . Applying the same fitting procedure to fully simulated events generated with the values  $\Delta m_d = 0.475 \text{ ps}^{-1}$  and  $\epsilon_b^Q = 0.689$  as a further cross-check gave:

$$\Delta m_d = 0.490 \pm 0.027 \text{ ps}^{-1}, \quad \epsilon_b^Q = 0.693 \pm 0.004 \quad (\text{full simulation}). \quad (25)$$

### 6.3.3 Systematic uncertainties

The following systematic uncertainties, summarised in Tab. 4, were studied.

- *Production rates of B hadrons.*

Following the procedure described in [15], the values of  $\bar{\chi}$ ,  $\chi_d$  and  $f_{b\text{-baryon}}$  were varied independently by their measured errors, giving correlated variations of  $f_d$  and  $f_s$  and consequently of  $F_{B_d}$  and  $F_{B_s}$ . The quantities  $\chi_d$  and  $\Delta m_d$  are related by equation 7. This correlation is taken into account below in the combination of the  $\Delta m_d$  results from the different analyses (Sect. 7).

- *B meson lifetimes.*

The central values and uncertainties given in Tab. 1 were used.

- *Fractions of leptons.*

A relative variation of  $\pm 20\%$ , corresponding to the accuracy of the measurement of the fake lepton rate in the data, was applied to the fraction of fake leptons, leptons from charm and cascade semileptonic decays. These variations were compensated by a corresponding variation of the fraction of direct leptons. This variation takes into account the systematic uncertainties coming from different semileptonic B decay models.

- *Tagging purities :  $\epsilon_c^{like}, \epsilon_h^{like}$ .*

Absolute variations of  $\pm 2\%$  were applied to the values of the tagging purities obtained from the simulation for events containing a fake lepton or a lepton from charm. These variations are similar to the deviations observed between the fitted value of  $\epsilon_b^Q$  in the data as compared to the nominal value expected from the simulation. Simulation samples, which correspond to different detector configurations and different tuning of the relevant parameters, were used to check the stability of the values used for the tagging purities. The difference between the values obtained does not exceed 0.5 %.

- *Fraction of  $\overline{B}_d^0$  in cascade decays.*

In simulated events, the fraction of  $\overline{B}_d^0$  in direct semileptonic decays is 39.2% and it is 46% in cascade decays. In the fitting procedure, the fraction of  $\overline{B}_d^0$  in cascade semileptonic decays was taken equal to  $(46 \pm 10)\%$ , and this variation was compensated by a change in the corresponding fraction of  $B^-$  mesons.

- *Control of the accuracy on the time measurement.*

This was evaluated from the residual difference between data and simulation in the reconstructed B energy and decay length distributions. Details of the procedure are given in [15].

In the  $\ell - Q_{hem}$  channel, the measured mass difference between the two physical  $B_d^0$  states is then:

$$\Delta m_d = 0.493 \pm 0.042 \pm 0.027 \text{ ps}^{-1}. \quad (26)$$

## 6.4 Measurement of $\Delta m_d$ using an inclusive reconstruction of $D^{*\pm}$ mesons

In this analysis method, events with an identified high  $p_t$  lepton accompanied by a  $D^{*\pm}$  of opposite charge, present in the same jet, are selected. As in the previous analysis, the lepton determines the decay sign and the production sign is determined from the hemisphere charge in the opposite hemisphere. The  $D^{*\pm}$  are identified by an inclusive method, based on the small  $Q$  value in the  $D^{*+} \rightarrow D^0 \pi^+$  decay, which allows the slow  $\pi^+$  from that decay to be identified. The identification of the  $D^{*\pm}$ , and the fact that the lepton and  $\pi^+$  are of opposite sign in the signal events, provides a much purer sample than in the other inclusive analyses and allows the combinatorial background to be studied.

### 6.4.1 Inclusive search for $D^{*\pm}$ candidates

The analysis is based on the identification of  $D^{*+} \rightarrow D^0 \pi^+$  in semileptonic decays of B hadrons. This identification is performed in an inclusive way, by reconstructing a B hadron secondary vertex corresponding to the  $D^{*\pm}$ -lepton system as was described in Sect. 6.1, and by finding the charged  $\pi$  from the  $D^{*\pm}$  decay, called  $\pi^*$  in the following. A detailed description of the method used can be found in [15]. The  $\pi^*$  candidate was searched for among all the particles belonging to the jet, excluding the lepton candidate, by computing the difference between the masses of two sets of particles. If the  $\pi^*$  was one of the B decay product candidates the following mass difference was evaluated:

$$\Delta M = M(\text{All B decay products}) - M(\text{All B decay products except the } \pi^*). \quad (27)$$

If the  $\pi^*$  was not one of the B decay product candidates, the evaluated mass difference was:

$$\Delta M = M(\text{All B decay products plus the } \pi^*) - M(\text{All B decay products}) \quad (28)$$

In the calculation of the above masses, the lepton candidate was always excluded. Two classes of events were defined according to the relative charges of the  $\pi^*$  and the lepton. A semileptonic  $B_d^0$  decay should produce a lepton and a  $\pi^*$  of opposite charge. For this reason, opposite charge pairs define right sign events, while same charge pairs, expected from the background sources, define wrong-sign events. Fig. 6 shows the  $\Delta M$  distribution for right- and wrong-sign events. An excess of right-sign events at low mass difference is clearly seen. The level of the combinatorial background at the given value of  $\Delta M$  was obtained from the data, using the wrong-sign distribution multiplied by the ratio between the numbers of right- and wrong-sign combinatorial background candidates observed in the simulation at the same value of  $\Delta M$  :

$$N_{comb}^{right-sign}(data) = N_{comb}^{wrong-sign}(data) \frac{N_{comb}^{right-sign}(sim.)}{N_{comb}^{wrong-sign}(sim.)} \quad (29)$$

In this expression, simulated events with a  $\pi^*$  candidate really coming from a charged  $D^*$  decay were removed to obtain  $N_{comb}^{right-sign}(sim.)$ . For the measurement of  $\overline{B}_d^0 - \overline{B}_d^0$  oscillations, events with  $\Delta M$  between 0.14 and 0.16 GeV/ $c^2$  were selected. In this interval, the fraction of events from the combinatorial background evaluated using equation (29) was  $f_{comb} = (30.6 \pm 1.5)\%$ . After background subtraction there were  $4135 \pm 100$   $D^*$  candidates in the selected region and, as explained in [15],  $3523 \pm 150$  of them can be attributed to  $\overline{B}_d^0$  decays.

#### 6.4.2 Measurement of $\Delta m_d$

The same method as that applied to the  $\ell - Q_{hem}$  analysis was used. The main difference concerned the evaluation of the different components entering into the likelihood function. Events in the  $\pi^*$  signal and in the combinatorial background were considered separately:

$$\mathcal{P}^{like}(t) = (1 - f_{comb})\mathcal{P}_{\pi^*}^{like}(t) + f_{comb}\mathcal{P}_{comb}^{like}(t) \quad (30)$$

and similarly for  $\mathcal{P}^{unlike}(t)$ . For events in the  $\pi^*$  signal:

$$\begin{aligned} \mathcal{P}_{\pi^*}^{like}(t) &= f_B^{\pi^*} [ F_{B_d}^{\pi^*} ((\epsilon_b^Q \mathcal{P}_{B_d}^{mix.}(t') + (1 - \epsilon_b^Q) \mathcal{P}_{B_d}^{unmix.}(t')) \otimes \mathcal{R}_B^{\pi^*}(t' - t)) \\ &\quad + F_{B_u}^{\pi^*} (1 - \epsilon_b^Q) (\mathcal{P}_{B_u}(t') \otimes \mathcal{R}_B^{\pi^*}(t' - t)) \\ &\quad + F_{B_s}^{\pi^*} ((\epsilon_b^Q \mathcal{P}_{B_s}^{mix.}(t') + (1 - \epsilon_b^Q) \mathcal{P}_{B_s}^{unmix.}(t')) \otimes \mathcal{R}_B^{\pi^*}(t' - t)) ] \\ &\quad + (1 - f_B^{\pi^*}) \epsilon_{back.}^{like} \mathcal{P}_{back.}(t) \end{aligned} \quad (31)$$

and

$$\begin{aligned} \mathcal{P}_{\pi^*}^{unlike}(t) &= f_B^{\pi^*} [ F_{B_d}^{\pi^*} (((1 - \epsilon_b^Q) \mathcal{P}_{B_d}^{mix.}(t') + \epsilon_b^Q \mathcal{P}_{B_d}^{unmix.}(t')) \otimes \mathcal{R}_B^{\pi^*}(t' - t)) \\ &\quad + F_{B_u}^{\pi^*} \epsilon_b^Q (\mathcal{P}_{B_u}(t') \otimes \mathcal{R}_B^{\pi^*}(t' - t)) \\ &\quad + F_{B_s}^{\pi^*} (((1 - \epsilon_b^Q) \mathcal{P}_{B_s}^{mix.}(t') + \epsilon_b^Q \mathcal{P}_{B_s}^{unmix.}(t')) \otimes \mathcal{R}_B^{\pi^*}(t' - t)) ] \\ &\quad + (1 - f_B^{\pi^*}) (1 - \epsilon_{back.}^{like}) \mathcal{P}_{back.}(t) \end{aligned} \quad (32)$$

where  $f_B^{\pi^*}$  is the fraction of events with a high  $p_t$  lepton from a direct semileptonic B hadron decay, and  $F_{B_d}^{\pi^*}$ ,  $F_{B_u}^{\pi^*}$  and  $F_{B_s}^{\pi^*}$  are the respective fractions of events from  $\overline{B}_d^0$ ,  $B^-$  and  $\overline{B}_s^0$  inside this category.

These fractions  $F_{B_q}^{\pi^*}$  are given by the relative production rates of different B hadrons in a  $b$  quark jet and the relative production rates of charged  $D^{*+}$  in their semileptonic decays. Apart from the  $\overline{B}_d^0$ , which has a relatively large decay rate through the exclusive channel  $\overline{B}_d^0 \rightarrow D^{*+} \ell \overline{\nu}_\ell$ , the other contributions originate from  $D^{**}$  decays. Their values were normalized to the acceptance for the exclusive channel  $\overline{B}_d^0 \rightarrow D^{*+} \ell \overline{\nu}_\ell$ . They are [15]:

$$F_{B_u}^{\pi^*} = (15.4 \pm 3.9)\%, \quad (33)$$

$$F_{B_s}^{\pi^*} = (1.4 \pm 1.4)\%, \quad (34)$$

and therefore

$$F_{B_d}^{\pi^*} = 1 - F_{B_u}^{\pi^*} - F_{B_s}^{\pi^*} = (83.2 \pm 4.1)\%. \quad (35)$$

The value of  $F_{B_d}^{\pi^*}$  includes the expected fraction of charged  $D^{*\pm}$  produced in  $D^{**}$  decays,  $(7.4 \pm 1.4)\%$  [15]. No significant contribution was expected from  $b$  baryon semileptonic decays, so they were neglected.

According to the simulation, leptons from cascade decays give only a small contribution,  $f_{bc}^\ell = (1.0 \pm 0.1)\%$ , since their contribution is suppressed by about an order of magnitude because cascade decays in the right-sign sample have to originate from mechanisms with two D mesons produced in the decay of the B hadron. Events in which the lepton is emitted by the D produced in the  $D^{*+}$  decay contribute to the wrong sign sample.

Leptons from semileptonic decays of D hadrons in  $Z^0 \rightarrow c\bar{c}$  events contribute only to the wrong-sign sample.

The contribution from fake leptons is also expected to be reduced as compared to their rate in the inclusive lepton sample because they have to originate from  $Z^0 \rightarrow c\bar{c}$  or  $\rightarrow b\bar{b}$  events only. The fraction of fake leptons,  $f_h^\ell = (2.8 \pm 0.2)\%$ , was considered simultaneously with the cascade contribution, giving:

$$1 - f_B^{\pi^*} = f_h^\ell + f_{bc}^\ell = (3.8 \pm 0.2)\%. \quad (36)$$

As their relative fraction is smaller than in the  $\ell - Q_{hem}$  analysis, all events in which the lepton was not from a direct semileptonic decay of a B hadron were considered together. This included events with a fake lepton, which was the main component, and events from charm and cascade decays. Their decay time distribution,  $\mathcal{P}_{back.}(t)$ , was taken from the simulation, as well as their tagging purity using the hemisphere charge,  $\epsilon_{back.}^{like} = 0.44$ .

Similar expressions as for  $\mathcal{P}_{\pi^*}^{like(unlike)}(t)$  were derived for events in the combinatorial background, i.e. for  $\mathcal{P}_{comb}^{like}(t)$  and  $\mathcal{P}_{comb}^{unlike}(t)$ . The fraction of these events,  $f_{comb}$ , was evaluated to be  $0.300 \pm 0.018$  [15]. For these events, different time resolution functions,  $\mathcal{R}_B^{comb}(t' - t)$ , were obtained from the simulation. In the combinatorial background, the relative fractions of direct leptons from the different types of B hadrons,  $F_{B_q}^{comb}$ , are given by the usual production rates of B hadrons in jets:  $F_{B_q}^{comb} = f_q$ . Other sources of lepton candidates in the combinatorial background are:

- leptons from cascade decays with a fraction of 7%,
- leptons from charm semileptonic decays: 5%,
- fake leptons with a rate of 17.2%, which is larger than in the  $\ell - Q_{hem}$  analysis, mainly because a different lepton selection was used and also because there may be several  $\pi^* - \ell$  pair candidates.

The fraction of non-direct lepton candidates in the combinatorial background was thus evaluated to be  $(29.2 \pm 1.0)\%$ .

Using the above values, the values of  $\Delta m_d$  and  $\epsilon_b^Q$  which correspond to the maximum of the log-likelihood distribution were obtained:

$$\Delta m_d = 0.499 \pm 0.053 \text{ ps}^{-1}, \quad \epsilon_b^Q = 0.656 \pm 0.012. \quad (37)$$

The experimental distributions of the decay time for unlike and like-sign events are shown in Fig. 7, with the result of the fit superimposed. The experimental distribution of the fraction of like-sign events versus the decay time is shown in Fig. 8.

The same fitting procedure was repeated on simulated events, generated with the values  $\Delta m_d = 0.475 \text{ ps}^{-1}$  and  $\epsilon_b^Q = 0.691$ , and gave:

$$\Delta m_d = 0.507 \pm 0.028 \text{ ps}^{-1}, \quad \epsilon_b^Q = 0.699 \pm 0.007 \quad (simulation) \quad (38)$$

On dedicated samples of simulated events containing only pure  $\overline{B}_d^0 \rightarrow D^{*+} \ell \overline{\nu}_\ell$  decays, the corresponding result was:

$$\Delta m_d = 0.487 \pm 0.016 \text{ ps}^{-1}, \quad \epsilon_b^Q = 0.693 \pm 0.006 \quad (simulation) \quad (39)$$

### 6.4.3 Systematic uncertainties

Various sources of systematic uncertainties were considered. The most relevant of them are reported in Tab. 5.

- *Fraction of  $\overline{B}_d^0$  in the  $\pi^*$  signal,  $F_{B_d}^{\pi^*}$ .*  
The uncertainty on this parameter depends on the corresponding error on the  $D^{**}$  production rate in B hadron semileptonic decays.
- *Uncertainty on the level of the combinatorial background.*  
This was discussed in the previous subsection.
- *Fraction of direct leptons from B decays in the signal.*  
The level of fake leptons and of leptons from cascade decays, in the  $\pi^*$  signal, is reduced by about an order of magnitude compared to the inclusive lepton analysis. Thus, only a very small effect is expected from this source.
- *Fraction of  $B_d^0$  in the combinatorial background,  $\epsilon_{B_d}^{comb}$ .*  
The main uncertainty on  $\epsilon_{B_d}^{comb}$ , which is equivalent to  $f_d$ , comes from the knowledge of  $b$  baryon production in jets,  $f_{b\text{-baryon}}$ , as noticed in the  $\ell - Q_{hem}$  analysis.
- *Lifetime difference between the  $\overline{B}_d^0$  and all B hadrons.*  
A variation of  $\pm 0.05$  ps on the  $B_d^0$  lifetime was used.
- *Rate of fake leptons.*  
As noticed, this is expected to be larger than observed in the  $\ell - Q_{hem}$  analysis, and rather conservative uncertainties were used.
- *Tagging purity for fake leptons.*  
The central value is taken from the simulation and a conservative uncertainty was used.
- *Control of the time measurement.*  
The procedure was explained in [15].

In the  $(\pi^* - \ell) - Q_{hem}$  channel, the measured mass difference between the two physical  $B_d^0$  states is then:

$$\Delta m_d = 0.499 \pm 0.053 \pm 0.015 \text{ ps}^{-1}. \quad (40)$$

## 6.5 The lepton-lepton channel

In this measurement, the decay sign was determined from the lepton in one hemisphere, provided a secondary vertex was reconstructed including that lepton, and the production sign was determined from the lepton in the opposite hemisphere.

### 6.5.1 Event selection

This analysis, despite the reduced statistics compared with the  $\ell - Q_{hem}$  analysis, profits from the better purity of the  $b$  charge determination from the presence of a pair of high  $p_t$  leptons.

The lepton selection described in 6.3.1 was used, except that the  $p_t$  cut was slightly modified in order to increase the efficiency. In a lepton jet, the sum of the energies of all those particles whose directions were nearer to the lepton than to the jet direction,  $E_{sub}$ , was expected to be smaller for events from direct  $b$  semileptonic decay than for the other sources of final state leptons. An optimization of the efficiency versus charge purity was obtained by a two dimensional cut in the  $p_t - E_{sub}$  plane. An event was selected if at least one lepton per hemisphere passed this cut.

The double lepton tag has the additional advantage of reducing the non- $b$  background. As a consequence, the fractions of lepton candidates in the classes of simulated events defined previously were:

$$f_b^\ell = 82.5\%, \quad f_{bc}^\ell = 11.4\%, \quad f_c^\ell = 4.7\%, \quad f_h^\ell = 1.4\%. \quad (41)$$

### 6.5.2 Measurement of $\Delta m_d$

In both hemispheres of the selected events, the secondary vertex search was performed as explained in Sect. 6.1. Only events having at least one reconstructed secondary vertex were used to measure  $\Delta m_d$ . They were classified as mixed if the charge of the two leptons was the same, and as unmixed if they were different. The numbers of events classified as mixed and unmixed were 1579 and 3199 respectively.

If only one hemisphere had a reconstructed secondary vertex with a corresponding measured proper time  $t$ , the probabilities of obtaining such a time were expressed by equations (18) and (19), using appropriate values for  $\epsilon_x^{tag}$ . In particular

$$\begin{aligned} \epsilon_b^Q &= \sum_q F_{B_q} \epsilon_{B_q}^\ell (1 - \mathcal{P}_{B_q}^{mix.}(t') \otimes \mathcal{R}_B(t' - t)) \\ &+ \sum_q F_{B_q} (1 - \epsilon_{B_q}^\ell) \mathcal{P}_{B_q}^{mix.}(t') \otimes \mathcal{R}_B(t' - t). \end{aligned} \quad (42)$$

The integrals in this expression are null for charged B mesons and  $b$  baryons and correspond to the time integrated probabilities for mixing  $\chi_q = \frac{x_q^2}{2(1+x_q^2)}$  for neutral B mesons (here  $q = d, s$ ). Therefore  $\epsilon_b^Q$  is implicitly a function of  $\Delta m_d$ , so the hemisphere without time measurement also provides information on  $\Delta m_d$ . In (18) and (19),  $\epsilon_c^{like}$  and  $\epsilon_h^{like}$  refer to the total probabilities of classifying charm and combinatorial background events as mixed. Their values here, taken from the simulation, are  $\epsilon_c^{like} = 18\%$  and  $\epsilon_h^{like} = 49\%$ .

The events with a reconstructed secondary vertex on each hemisphere had two measured proper times,  $t_1$  and  $t_2$ , and the probabilities of being classified as mixed or unmixed were expressed as functions of both times:

$$\begin{aligned} \mathcal{P}^{like}(t_1, t_2) &= \\ &f_b \sum_q F_{B_q} (\epsilon_{B_q}^\ell \mathcal{P}_{B_q}^{mix.}(t'_1) \otimes \mathcal{R}_B(t'_1 - t_1) + (1 - \epsilon_{B_q}^\ell) \mathcal{P}_{B_q}^{unmix.}(t'_1) \otimes \mathcal{R}_{BC}(t'_1 - t_1)) \\ &\quad \sum_q F_{B_q} (\epsilon_{B_q}^\ell \mathcal{P}_{B_q}^{unmix.}(t'_2) \otimes \mathcal{R}_B(t'_2 - t_2) + (1 - \epsilon_{B_q}^\ell) \mathcal{P}_{B_q}^{mix.}(t'_2) \otimes \mathcal{R}_{BC}(t'_2 - t_2)) \\ &+ f_b \sum_q F_{B_q} (\epsilon_{B_q}^\ell \mathcal{P}_{B_q}^{unmix.}(t'_1) \otimes \mathcal{R}_B(t'_1 - t_1) + (1 - \epsilon_{B_q}^\ell) \mathcal{P}_{B_q}^{mix.}(t'_1) \otimes \mathcal{R}_{BC}(t'_1 - t_1)) \\ &\quad \sum_q F_{B_q} (\epsilon_{B_q}^\ell \mathcal{P}_{B_q}^{mix.}(t'_2) \otimes \mathcal{R}_B(t'_2 - t_2) + (1 - \epsilon_{B_q}^\ell) \mathcal{P}_{B_q}^{unmix.}(t'_2) \otimes \mathcal{R}_{BC}(t'_2 - t_2)) \\ &+ f_c \epsilon_c^{like} \mathcal{P}_C(t_1) \mathcal{P}_C(t_2) \\ &+ f_h \epsilon_h^{like} \mathcal{P}_H(t_1) \mathcal{P}_H(t_2) \end{aligned} \quad (43)$$

The function  $\mathcal{P}^{unlike}(t_1, t_2)$  was obtained from this formula by appropriately replacing  $\mathcal{P}_{B_q}^{unmix.}(t')$ ,  $\epsilon_c^{like}$ , and  $\epsilon_h^{like}$  in a single hemisphere by  $\mathcal{P}_{B_q}^{mix.}(t')$ ,  $(1 - \epsilon_c^{like})$ , and  $(1 - \epsilon_h^{like})$  respectively, and vice-versa.

The distribution to be minimized as a function of the parameter  $\Delta m_d$  was then the sum of two parts:

$$\mathcal{L}_{single} = - \sum_{like-sign\ events}^{single} \ln(\mathcal{P}^{like}(t)) - \sum_{unlike-sign\ events}^{single} \ln(\mathcal{P}^{unlike}(t)) \quad (44)$$

and

$$\mathcal{L}_{double} = - \sum_{like-sign\ events}^{double} \ln(\mathcal{P}^{like}(t_1, t_2)) - \sum_{unlike-sign\ events}^{double} \ln(\mathcal{P}^{unlike}(t_1, t_2)), \quad (45)$$



where the first expression is a sum over events with only one measured time and the latter is a sum over events with two measured times.

The value of  $\Delta m_d$  corresponding to the maximum log-likelihood was found to be :

$$\Delta m_d = 0.480 \pm 0.040 \text{ ps}^{-1}. \quad (46)$$

The experimental distributions of the decay time for like and unlike-sign events are shown in Fig. 9, with the result of the fit superimposed. A projection on a single time axis of the time distribution for the mixed event fraction is shown in Fig. 10.

The same fitting procedure was repeated on simulated events generated with  $\Delta m_d = 0.475$ , giving:

$$\Delta m_d = 0.450 \pm 0.040 \text{ ps}^{-1} \text{ (simulation)}. \quad (47)$$

### 6.5.3 Systematic uncertainties

The study of systematic uncertainties attached to this measurement is similar to that described for the  $\ell - Q_{hem}$  channel. However, since the maximum likelihood fit was a function of  $\Delta m_d$  only, the effect of the same variations of the parameters as summarized in Tab. 4 were different. This was particularly true for the variation of  $f_{bc}^\ell$  which, in the  $\ell - Q_{hem}$  channel, was partially compensated by a variation of the fitted value of  $\epsilon_b^Q$ . In this analysis, the contribution from the variation of  $f_{bc}^\ell$  to the systematic error on  $\Delta m_d$  was the most relevant one, as can be seen from Tab. 6, where its contribution is summarized in the total wrong charge rate  $\sum_q (1 - \epsilon_{B_q}^\ell)$ . The total systematic uncertainty on the measurement of  $\Delta m_d$  for the  $\ell - \ell$  channel was found to be  $\pm 0.051 \text{ ps}^{-1}$ , so that in this channel the measured mass difference between the two physical  $B_d^0$  states is

$$\Delta m_d = 0.480 \pm 0.040 \pm 0.051 \text{ ps}^{-1}. \quad (48)$$

## 7 Combined result

The four results given above were not from completely independent samples. In fact, while the overlap between the  $D^{*\pm} - Q_{hem}$  channel and the other samples is negligible, the lepton-lepton channel and the  $\pi^* - \ell$  samples are almost entirely contained in the  $\ell - Q_{hem}$  one. If the  $\pi^* - \ell$  candidates were removed from the  $\ell - Q_{hem}$  sample, the composition of the resulting sample would no longer be universal, as assumed previously, because they are enriched in  $B_d^0$  decays. Consequently, additional systematic uncertainties would have to be introduced, based on the simulation. Therefore, a different procedure was used to combine these measurements.

To write the error matrix, the statistical correlations between the samples were first estimated with simple hypotheses. Considering that the sensitivity to  $\Delta m_d$  of the different procedures was quite different (even with samples a factor 10 smaller, the lepton-lepton and  $\pi^* - \ell$  channels have statistical errors similar to the  $\ell - Q_{hem}$  channel), the effect of removing the small number of events used in the analysis with high sensitivity from the large sample analyzed with lower sensitivity was found to be quite small. In more detail, calling  $\sigma_1$  and  $\sigma_2$  the errors obtained with two methods, the error  $\sigma_1^*$ , expected from the low sensitivity method once the smaller sample was removed, was evaluated by taking into account the different signal to noise ratios. Since the samples with corresponding errors  $\sigma_1^*$  and  $\sigma_2$  are uncorrelated, they can be combined to obtain an error  $\sigma_{comb}$  with

the usual weighting procedure. Imposing the condition

$$\frac{1}{\sigma_{comb}^2} = \left( \frac{1}{\sigma_1^2} + \frac{1}{\sigma_2^2} - \frac{2\rho}{\sigma_1\sigma_2} \right) \frac{1}{1 - \rho^2},$$

the equation can be solved for the correlation  $\rho$  between the two samples. All the correlation values were found to be below 20%. This evaluation was verified using the simulation, by removing common events and using the exact sample composition, which is known in this case. The systematic errors were then included in the error matrix by taking into account the common parts.

The stability of the result and of the estimated errors was checked by changing the correlations from the values obtained from the previous equation to the ones given by the Monte Carlo. The variations were found to be negligible.

The combined estimate for the mass difference between the two physical  $B_d^0$  mass eigenstates was thus found to be:

$$\Delta m_d = 0.496 \pm 0.034 \text{ ps}^{-1}, \quad (49)$$

based on the four evaluations described in this paper.

The value of  $\chi_d$  measured at the  $\Upsilon(4S)$  was used as an external parameter for the measurement of  $\Delta m_d$ , and  $\Delta m_d$  and  $\chi_d$  are related by equation (7). However, this correlation is important only for the  $(\ell - \ell)$  analysis, see Tab. 6. It was checked by an iterative procedure that the final result is stable with respect to the input  $\chi_d$  value.

## 8 Conclusion

Using data registered with the DELPHI detector between 1991 and 1994 and considering the correlation between *a)* the sign of a  $D^{*\pm}$  or of a lepton emitted at large  $p_t$  relative to its jet axis and *b)* either the sign of the weighted sum of charged particles produced in the opposite event hemisphere or that of a high  $p_t$  lepton in that hemisphere to define mixed and unmixed candidates, the mass difference between the  $B_d^0$  mass eigenstates was measured in four channels to be:

$$\begin{aligned} \Delta m_d &= 0.523 \pm 0.072 \pm 0.043 \text{ ps}^{-1} \quad (D^{*\pm} - Q_{hem}) \\ \Delta m_d &= 0.493 \pm 0.042 \pm 0.027 \text{ ps}^{-1} \quad (\ell - Q_{hem}) \\ \Delta m_d &= 0.499 \pm 0.053 \pm 0.015 \text{ ps}^{-1} \quad ((\pi^* - \ell) - Q_{hem}) \\ \Delta m_d &= 0.480 \pm 0.040 \pm 0.051 \text{ ps}^{-1} \quad (\ell - \ell). \end{aligned}$$

The combined result, taking into account statistical and systematic correlations between these measurements, is:

$$\Delta m_d = 0.496 \pm 0.034 \text{ ps}^{-1}.$$

This result supersedes all previous DELPHI measurements on  $\Delta m_d$ .

Using the value for the  $B_d^0$  lifetime given in Tab. 1, it also follows that :

$$\chi_d = 0.188 \pm 0.023.$$

## Acknowledgements

We are greatly indebted to our technical collaborators and to the funding agencies for their support in building and operating the DELPHI detector, and to the members of the CERN-SL Division for the excellent performance of the LEP collider.

## References

- [1] G. Altarelli and P.J. Franzini, Z. Phys. **C37** (1988) 271;  
P.J. Franzini, Phys. Rep. **173** (1989) 1.
- [2] CDF Coll., F. Abe et al., Phys. Rev. Lett. **74** (1995) 2626;  
D0 Coll., S. Abachi et al., Phys. Rev. Lett. **74** (1995) 2632.
- [3] A. J. Buras, MPI-PHT/95-17 (1995), hep-ph/9503262;  
A.J. Buras, M. Jasmin and P.H. Weisz Nucl. Phys. **B347** (1990) 491.
- [4] ARGUS Coll., H. Albrecht et al., Phys. Lett. **B 324** (1994) 249;  
CLEO Coll., J. Bartelt et al., Phys. Rev. **D50** (1994) 43.
- [5] ALEPH Coll., D. Decamp et al., Phys. Lett. **B284** (1992) 177;  
DELPHI Coll., P. Abreu et al., Phys. Lett. **B332** (1994) 488;  
L3 Coll., M. Acciarri et al., Phys. Lett. **B335** (1994) 542;  
OPAL Coll., R. Akers et al., Z. Phys. **C60** (1993) 199;  
UA1 Coll., C. Albajar et al., Phys. Lett. **B262** (1991) 171;  
CDF Coll., F. Abe et al., Phys. Rev. **D55** (1997) 2546.
- [6] ALEPH Coll., D. Buskulic et al., Phys. Lett. **B313** (1993) 498;  
ALEPH Coll., D. Buskulic et al., Phys. Lett. **B322** (1994) 441;  
ALEPH Coll., D. Buskulic et al., “Improved measurement of the  $B_d^0 - \bar{B}_d^0$  oscillation frequency”, CERN PPE/96-102, subm. to Z. Phys. **C**;  
DELPHI Coll., P. Abreu et al, Phys. Lett **B33** (1994) 409;  
DELPHI Coll., P. Abreu et al, Z. Phys **C72** (1996) 17;  
L3 Coll., M. Acciarri et al., Phys. Lett. **B383** (1996) 487;  
OPAL Coll., R. Akers et al., Phys. Lett. **B327** (1994) 411;  
OPAL Coll., R. Akers et al., Phys. Lett. **B336** (1994) 585;  
OPAL Coll., R. Akers et al., Z. Phys. **C66** (1995) 555;  
OPAL Coll., G. Alexander et al., Z. Phys. **C72** (1996) 377;  
OPAL Coll., K. Ackerstaff et al., “A Study of B Meson Oscillations Using Hadronic  $Z^0$  Decays Containing Leptons”, CERN-PPE/97-036, subm. to Z. Phys. **C**.
- [7] DELPHI Coll., P. Abreu et al., Nucl. Instr. and Meth. **A378** (1996) 57.
- [8] N. Binglefors et al., Nucl. Instr. and Meth. **A328** (1993) 447;  
V. Chabaud et al., Nucl. Instr. and Meth. **A368** (1996) 314.
- [9] E.G. Anassontzis et al., Nucl. Instr. and Meth. **A323** (1992) 351.
- [10] T. Sjöstrand, Comp. Phys. Comm. **82** (1994) 74.
- [11] N. Isgur, D. Scora, B. Grinstein and M. Wise, Phys. Rev. **D39** (1989) 799.
- [12] Particle Data Group, R. M. Barnett et al., Phys. Rev. **D54** (1996) 1.
- [13] ARGUS Coll., H. Albrecht et al., Phys. Lett. **B278** (1992) 202.
- [14] The LEP Electroweak Working Group and the SLD Heavy Flavor Group, “A Combination of Preliminary LEP and SLD Electroweak Measurements and Constraints on the Standard Model”, CERN PPE/96-183.
- [15] DELPHI Coll., P. Abreu et al., Z. Phys. **C74** (1997) 19;
- [16] ALEPH Coll., D. Buskulic et al., Phys. Lett. **B357** (1995) 699;  
DELPHI Coll., O. Podobrin and M. Feindt, “Inclusive Measurement of the  $b$  fragmentation function”, DELPHI 95-103 PHYS 538, contributed paper eps0560 to EPS-HEP95, Brussels, July 1995;  
OPAL Coll., G. Alexander et al., Phys. Lett. **B364** (1995) 93.
- [17] G.V. Borisov and C. Mariotti, Nucl. Instr. and Meth. **A372** (1996) 181.

Parameter	mean value and error	ref.
Inclusive B lifetime	$(1.549 \pm 0.020)$ ps	[12]
$B^+$ lifetime	$(1.62 \pm 0.06)$ ps	[12]
$B_d$ lifetime	$(1.56 \pm 0.06)$ ps	[12]
$B_s$ lifetime	$(1.61 \pm 0.10)$ ps	[12]
$b$ -baryon lifetime	$(1.14 \pm 0.08)$ ps	[12]
$\text{Br}(b \rightarrow \ell)$	$(11.13 \pm 0.29)\%$	[12]
$\text{Br}(b \rightarrow c \rightarrow \bar{\ell})$	$(7.9 \pm 0.8)\%$	[12]
$\text{Br}(b \rightarrow \bar{c} \rightarrow \ell)$	$(1.3 \pm 0.5)\%$	[12]
$\text{Br}(c \rightarrow \bar{\ell})$	$(9.5 \pm 0.9)\%$	[13]
$\bar{\chi}$	$0.1217 \pm 0.0046$	[14]
$\chi_d$	$0.175 \pm 0.016$	[12]
$Br_u^{**}$	$(1.0 \pm 0.2 \pm 0.1)\%$	[15]
$Br_d^{**}$	$(0.5 \pm 0.1 \pm 0.1)\%$	[15]
$Br_s^{**}$	$(0.4 \pm 0.4)\%$	[15]
$Br^*$	$(4.53 \pm 0.32)\%$	[15]
$\langle X_E \rangle$	$0.71 \pm 0.01$	[16]
$f_{b\text{-baryon}}$	$(8.7 \pm 2.9)\%$	[15]
$f_d$	$(40.5 \pm 2.0)\%$	(†)
$f_s$	$(10.2 \pm 2.0)\%$	(†)

Table 1: *Relevant parameters used in the analyses. The quantity  $Br^{**}$  is defined as the branching fraction for a B meson to decay into the  $D^{*(0,+)}X\ell^{-}\bar{\nu}_\ell$  final state with the  $D^{*(0,+)}X$  system originating from a  $D^{**}$  decay. The quantity  $Br^*$ , is the branching fraction of a B hadron into  $D^{*\pm}\ell^{-}\bar{\nu}_\ell$ .*

(†) *The values of  $f_d$  and  $f_s$  were determined following the procedure explained in [15] using  $\chi_s = 0.5$  and the values of  $\bar{\chi}$  and  $\chi_d$  given in the Table. The error on  $f_d$  is dominated by the uncertainty on  $f_{b\text{-baryon}}$ . The error on  $f_s$  receives similar contributions from the errors on  $\bar{\chi}$  and  $\chi_d$ .*

Decay mode	$\Delta M(\text{GeV}/c^2)$	Events	$f_{comb}$	$\epsilon_{comb}^{unlike}$	$r_{c\bar{c}}$
$K^- \pi^+$	0.1445 - 0.1465	2299	$0.324 \pm 0.030$	$0.489 \pm 0.007$	$0.34 \pm 0.04$
$K^- \pi^+ \pi^0$	0.1400 - 0.1520	2491	$0.450 \pm 0.050$	$0.509 \pm 0.011$	$0.40 \pm 0.05$
$K^- \pi^+ \pi^- \pi^+$	0.1440 - 0.1470	5192	$0.752 \pm 0.071$	$0.499 \pm 0.004$	$0.34 \pm 0.04$

Table 2: Values of the parameters used in the likelihood fit which are obtained from the data (see Sect. 5.4). The numbers of events quoted are after the requirement  $|Q_{hem}| > 0.1$ .

Contribution	variation of $\Delta m_d$ ( $\text{ps}^{-1}$ )
Time parametrization and $B$ momentum resolution	$\pm 0.020$
$B$ lifetime	$\mp 0.004$
$D$ lifetime	$\pm 0.001$
$B$ momentum parametrization	$\mp 0.007$
Fraction of charm events, $r_{c\bar{c}}$	$\pm 0.003$
Fraction of background, $f_{comb}$	$\pm 0.003$
Fraction of $B^\pm$ , $f_{B^\pm}$	$\pm 0.035$
$\epsilon_{comb}^{unlike}$	$\mp 0.005$
$\epsilon_{c\bar{c}}^{unlike}$	$\pm 0.005$
$\epsilon_{B^\pm}^{unlike}$	$\mp 0.011$
Total	$\pm 0.043$

Table 3: Systematic uncertainties for the  $D^{*\pm} - Q_{hem}$  channel. The sign ( $\pm$  or  $\mp$ ) of the error assigned to  $\Delta m_d$  shows the correlation with the variation of the different parameters.

Parameter	central value	range of variation	variation of $\Delta m_d$ (ps <sup>-1</sup> )
$\bar{\chi}$	0.1217	$\pm 0.0046$	$\pm 0.0005$
$\chi_d$	0.175	$\pm 0.016$	$\mp 0.0006$
$f_{b\text{-baryon}}$	0.087	$\pm 0.029$	$\pm 0.010$
$\langle \tau(\text{B}) \rangle$	1.549 ps	$\pm 0.020$ ps	$\mp 0.0008$
$\tau(\text{B}_d^0) / \langle \tau(\text{B}) \rangle$	1.007	$\pm 0.041$	$\mp 0.007$
$f_h^\ell$	10%	$\pm 2\%$	$\pm 0.010$
$f_{bc}^\ell$	8%	$\pm 2\%$	$\mp 0.007$
$f_c^\ell$	9.5%	$\pm 2.0\%$	$\pm 0.001$
$\epsilon_c^{like}$	37%	$\pm 2\%$	$\pm 0.009$
$\epsilon_h^{like}$	45%	$\pm 2\%$	$\pm 0.014$
$\text{B}_d^0$ cascade fraction	46%	$\pm 10\%$	$\pm 0.007$
control of $t$ measurement			$\pm 0.009$
Total			$\pm 0.027$

Table 4: Contributions to the systematic uncertainty on the measurement of  $\Delta m_d$ , in the  $\ell - Q_{hem}$  channel. The sign ( $\pm$  or  $\mp$ ) of the error assigned to  $\Delta m_d$  shows the correlation with the variation of the different parameters.

Parameter	central value	range of variation	variation of $\Delta m_d$ (ps <sup>-1</sup> )
$F_{B_d}^{\pi^*}$	0.832	$\pm 0.041$	$\mp 0.012$
$f_{comb}$	0.300	$\pm 0.018$	$\pm 0.001$
$f_{b\text{-baryon}}$	0.087	$\pm 0.029$	$\pm 0.002$
$\tau(\text{B}_d^0) / \langle \tau(\text{B}) \rangle$	1.007	$\pm 0.041$	$\mp 0.001$
$f_h^\ell$	0.292%	$\pm 0.010\%$	$\pm 0.002$
$\epsilon_h^{like}$	45%	$\pm 2\%$	$\pm 0.001$
control of $t$ measurement			$\pm 0.009$
Total			$\pm 0.015$

Table 5: Contributions to the systematic uncertainty on the measurement of  $\Delta m_d$  in the  $(\pi^* - \ell) - Q_{hem}$  channel. The sign ( $\pm$  or  $\mp$ ) of the error assigned to  $\Delta m_d$  shows the correlation with the variation of the different parameters.

Parameter	central value	range of variation	variation of $\Delta m_d$ (ps <sup>-1</sup> )
$\bar{\chi}$	0.1217	$\pm 0.0046$	$\mp 0.018$
$\chi_d$	0.175	$\pm 0.016$	+0.025 - 0.027
$f_{b\text{-baryon}}$	0.087	$\pm 0.029$	$\pm 0.005$
$\langle \tau(\mathbf{B}) \rangle$	1.549 ps	$\pm 0.020$ ps	$\mp 0.001$
$\tau(\mathbf{B}_d^0) / \langle \tau(\mathbf{B}) \rangle$	1.007	$\pm 0.041$	-0.017 + 0.014
$f_c^\ell, f_h^\ell$	0.047, 0.014	$\pm 15\%$	$\pm 0.004$
$\epsilon_c^{like}, \epsilon_h^{like}$	0.018, 0.018	$\pm 10\%$	-0.005 + 0.006
$\sum_q (1 - \epsilon_{B_q}^\ell)$	0.114	$\pm 6\%$	-0.030 + 0.032
control of $t$ measurement			$\pm 0.019$
Total			$\pm 0.051$

Table 6: Contributions to the systematic uncertainty on the measurement of  $\Delta m_d$  in the  $(\ell - \ell)$  channel. The sign ( $\pm$  or  $\mp$ ) of the error assigned to  $\Delta m_d$  shows the correlation with the variation of the different parameters.

# DELPHI

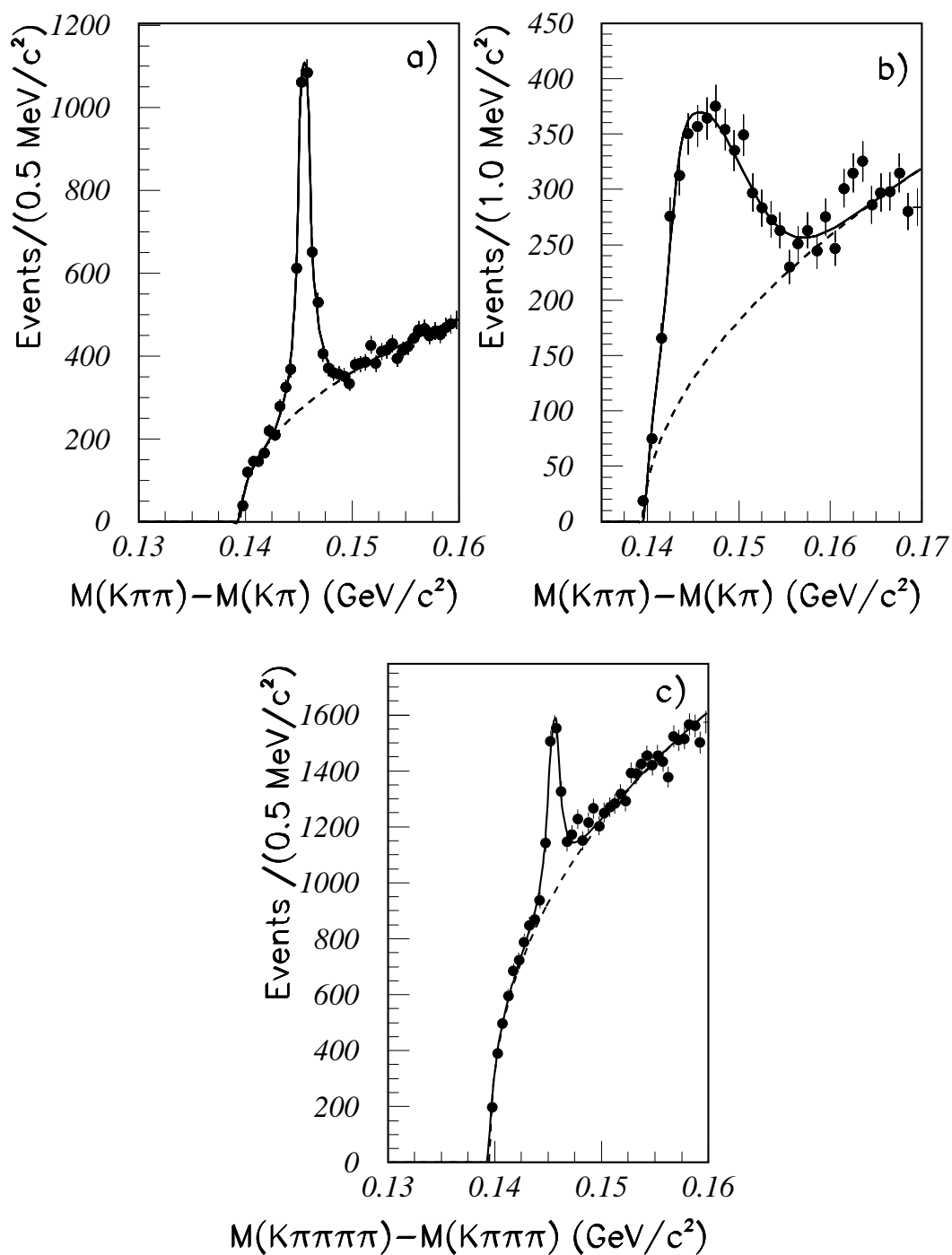


Figure 1: Distribution of  $\Delta M$  for a)  $K\pi$ , b)  $K\pi\pi^0$  and c)  $K\pi\pi\pi D^0$  decay candidates. The results of the fits, with signal and background shapes described in the text, are superimposed.



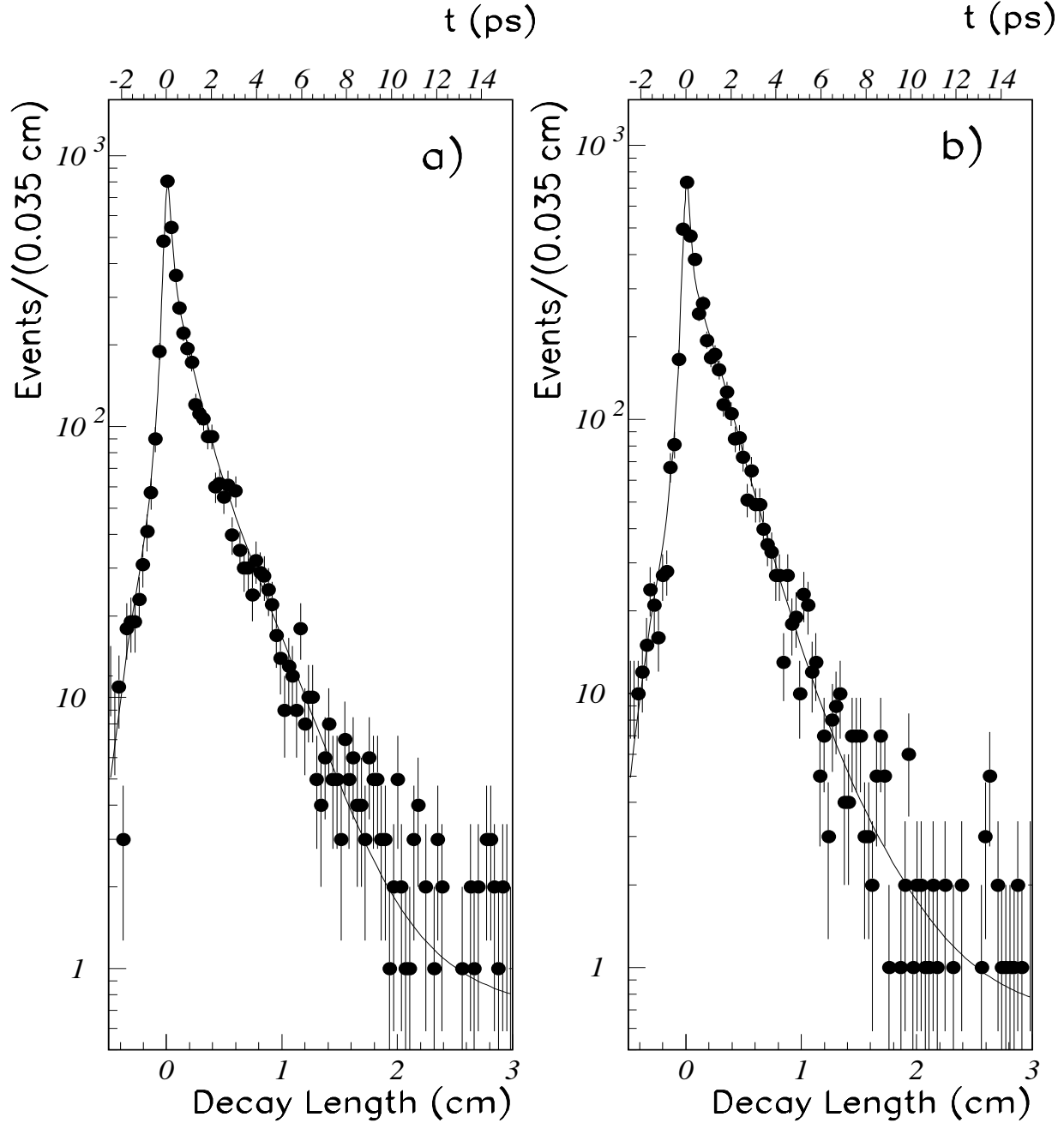


Figure 2: The distribution of the decay length for **a)** unlike-sign events and **b)** like-sign events in the  $D^{*\pm} - Q_{hem}$  channel. The dots with the error bars represent the data. The curve is the result of the fit. The equivalent range in the time variable  $t$  is given on the upper horizontal axis.

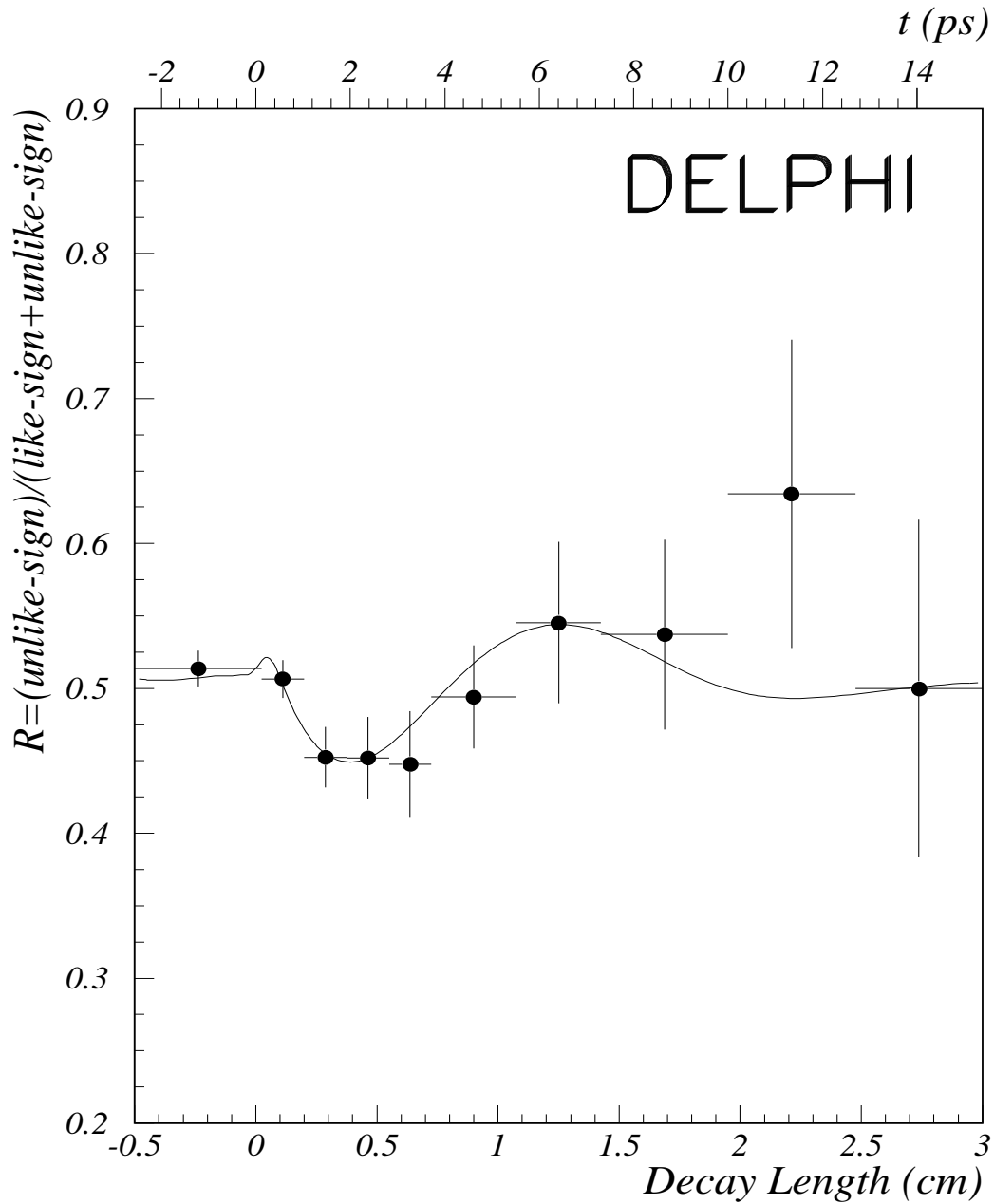


Figure 3: The fraction of unlike-sign events in the  $D^{*\pm} - Q_{hem}$  channel as a function of the decay length. The full dots with the error bars represent the data. The curve is the result of the fit. The equivalent range in the time variable  $t$  is given on the upper horizontal axis.

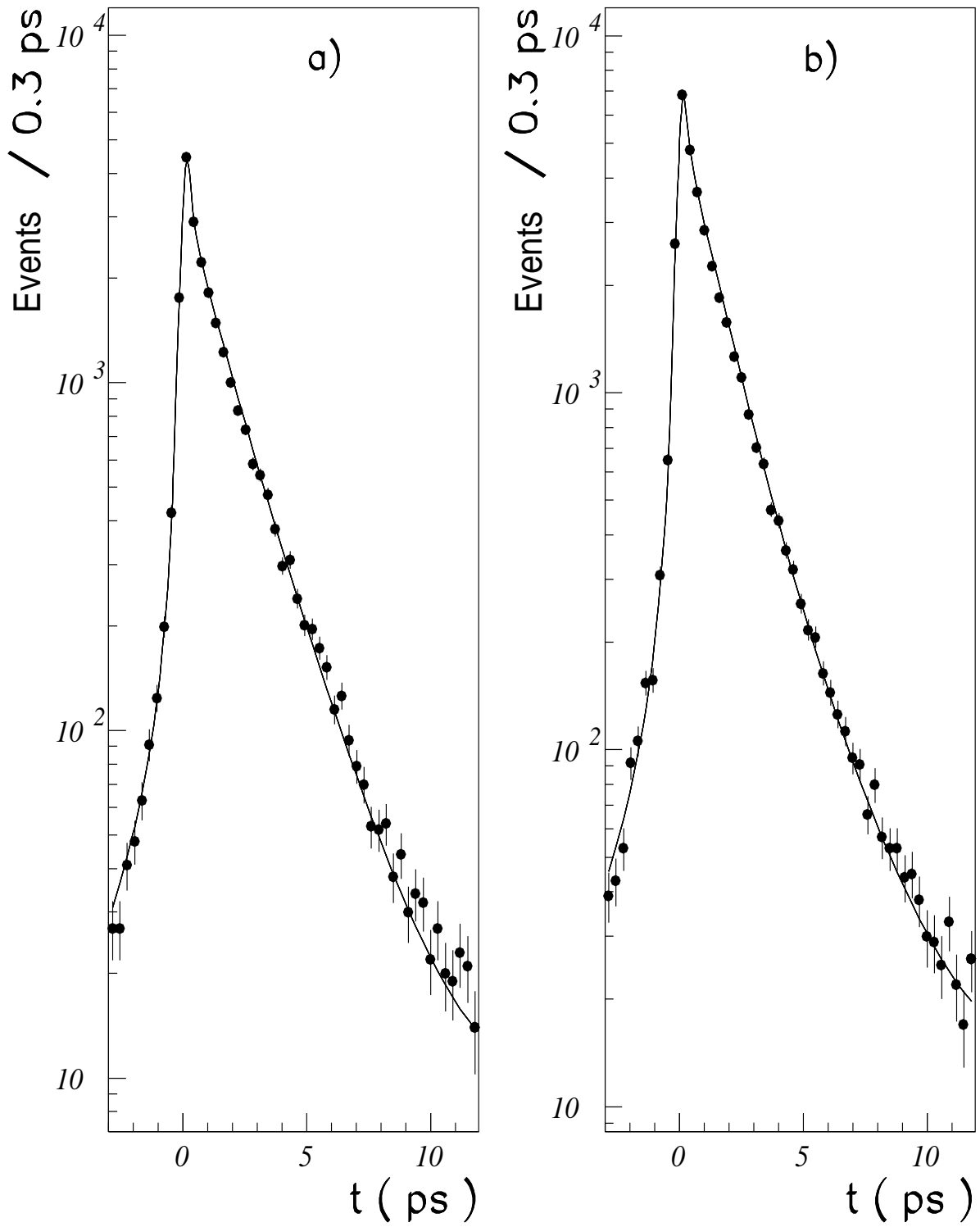


Figure 4: Time distributions for a) like-sign and b) unlike-sign events in the  $\ell - Q_{hem}$  channel. The curves are the result of the log-likelihood fit.

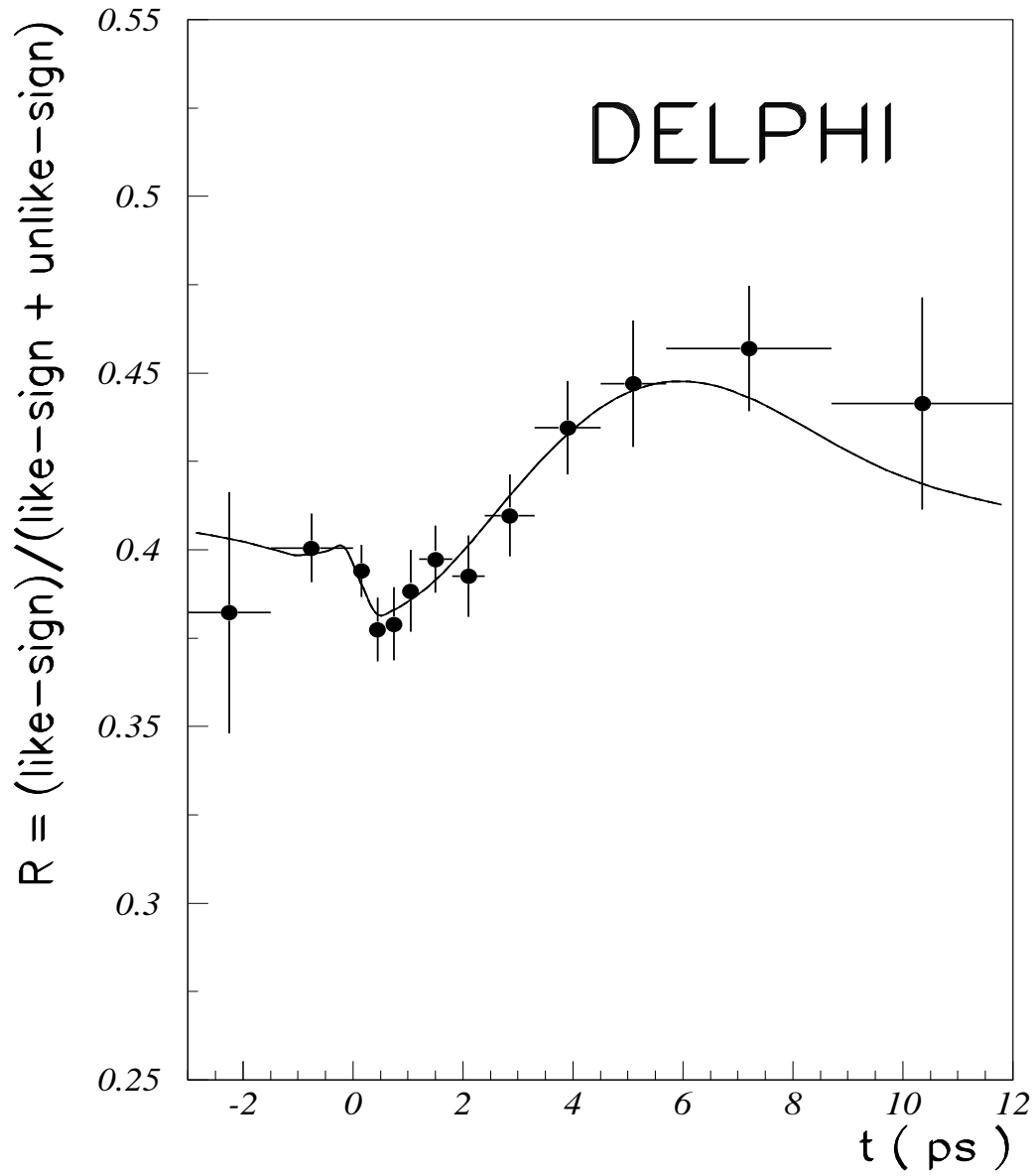


Figure 5: Time dependence of the fraction of like-sign events in the  $\ell - Q_{hem}$  channel. The curve is the result of the log-likelihood fit.

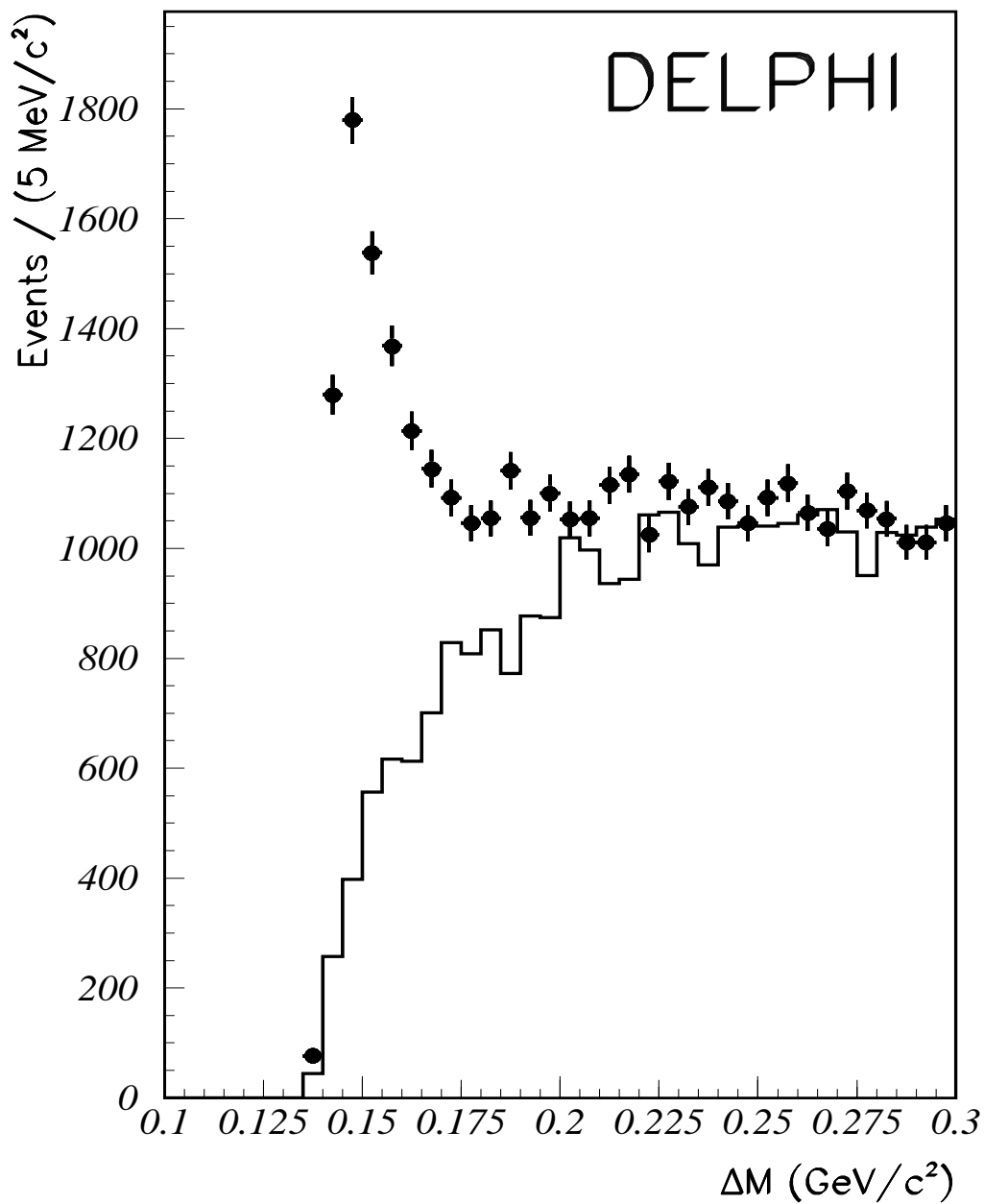


Figure 6:  $\Delta M$  distributions for 1991-1994 data. The points with the error bars represent the data. The histogram represents the distributions for wrong-sign combinations multiplied by the ratio of right-sign to wrong-sign measured in the simulation in each bin of the  $\Delta M$  variable.

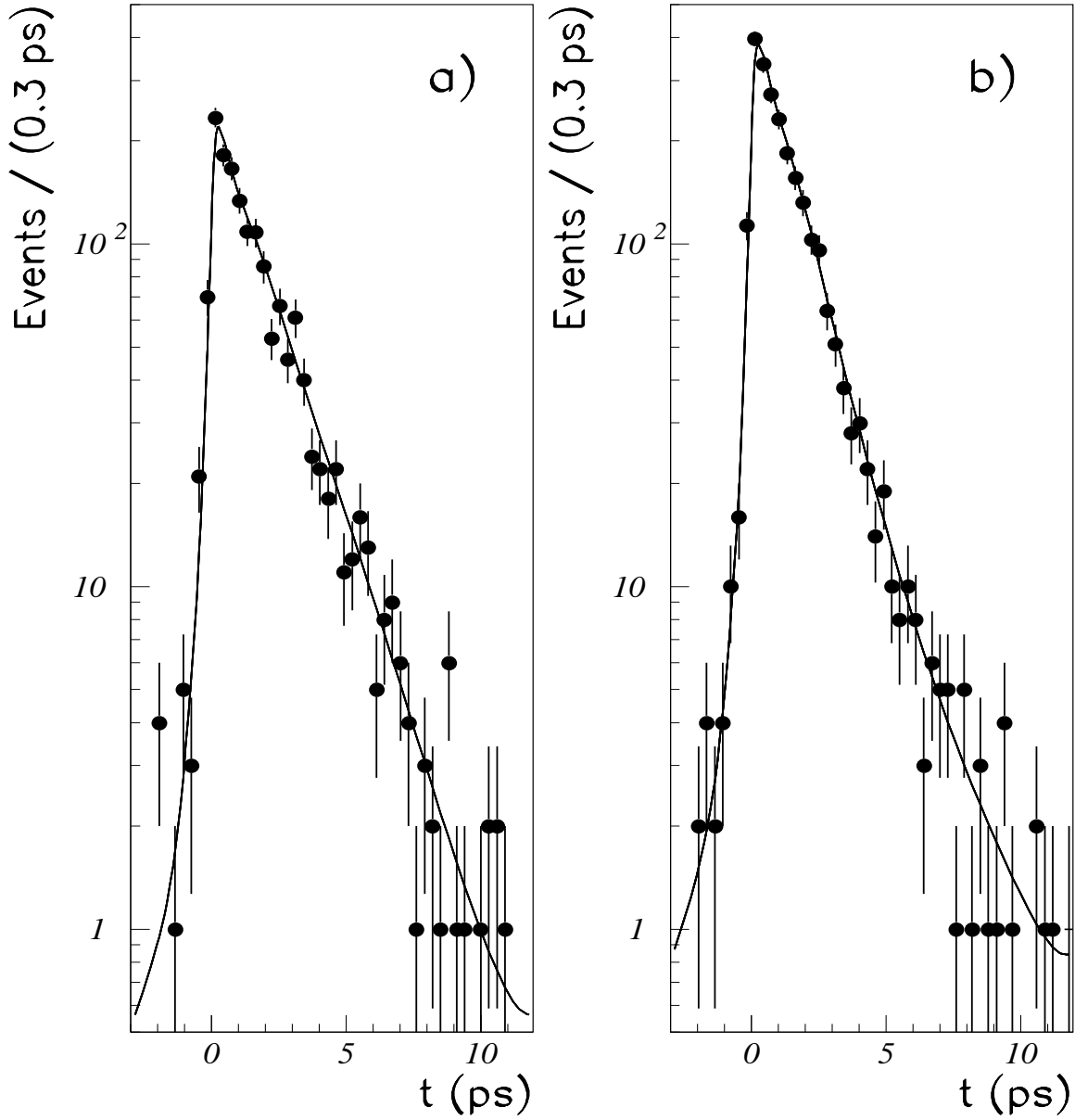


Figure 7: Time distributions for **a)** like-sign and **b)** unlike-sign events in the  $(\pi^*-\ell)-Q_{hem}$  analysis. The curves are the result of the log-likelihood fit.

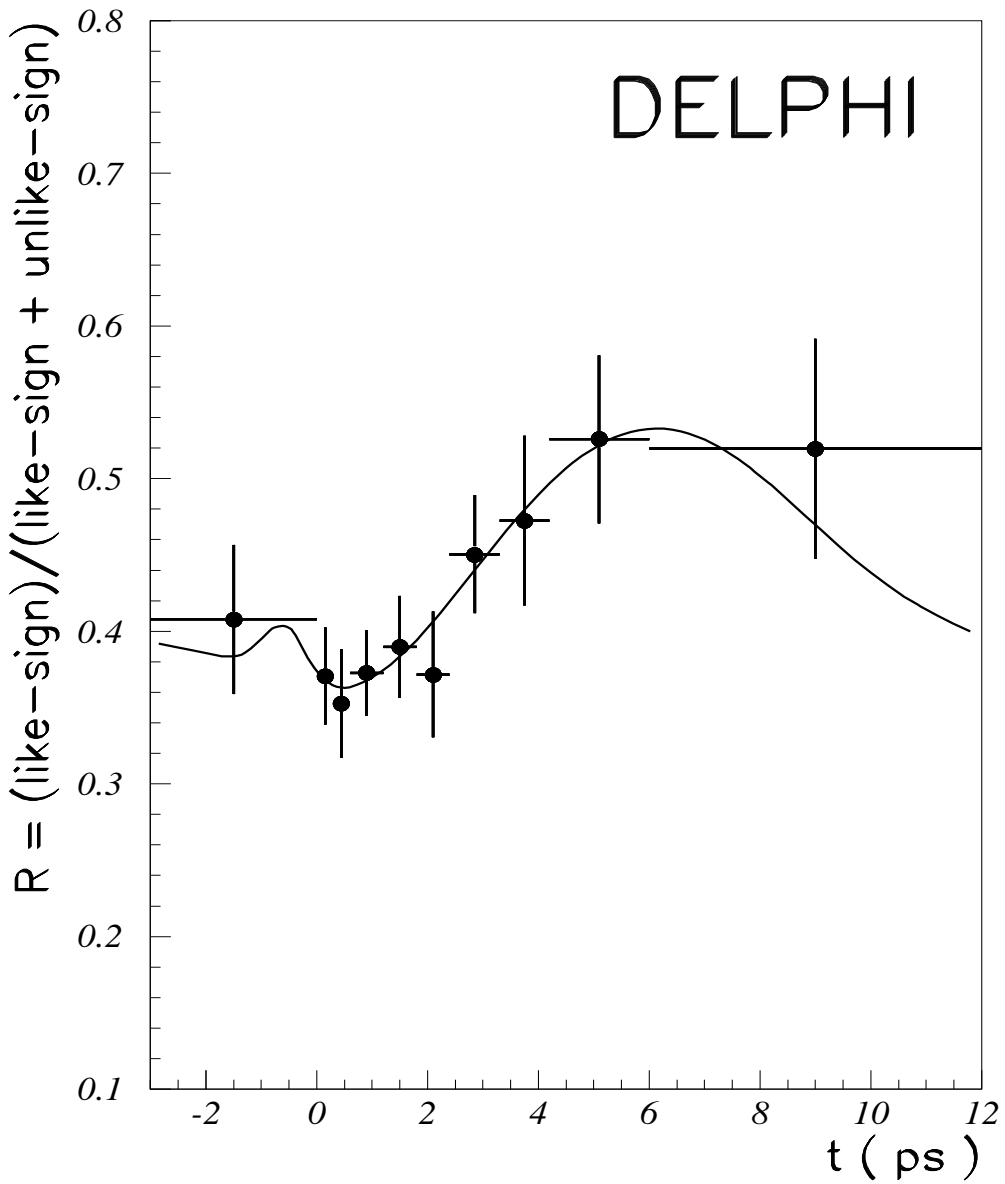


Figure 8: Time dependence of the fraction of like-sign events in the  $(\pi^* - \ell) - Q_{hem}$  channel. The curve is the result of the log-likelihood fit.

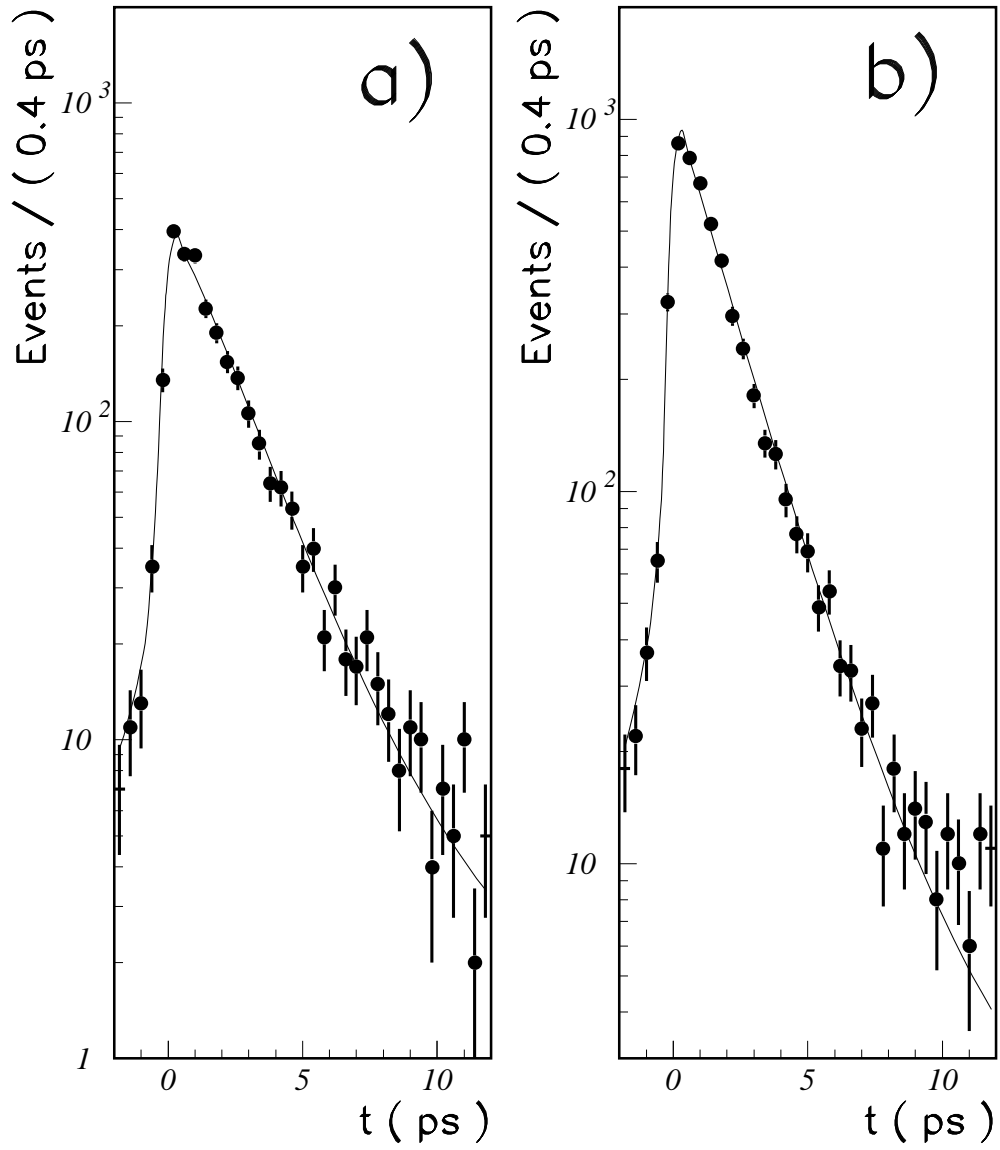


Figure 9: Time distributions for **a)** like-sign and **b)** unlike-sign events in the  $\ell-\ell$  channel. The curves are the result of the likelihood fit.



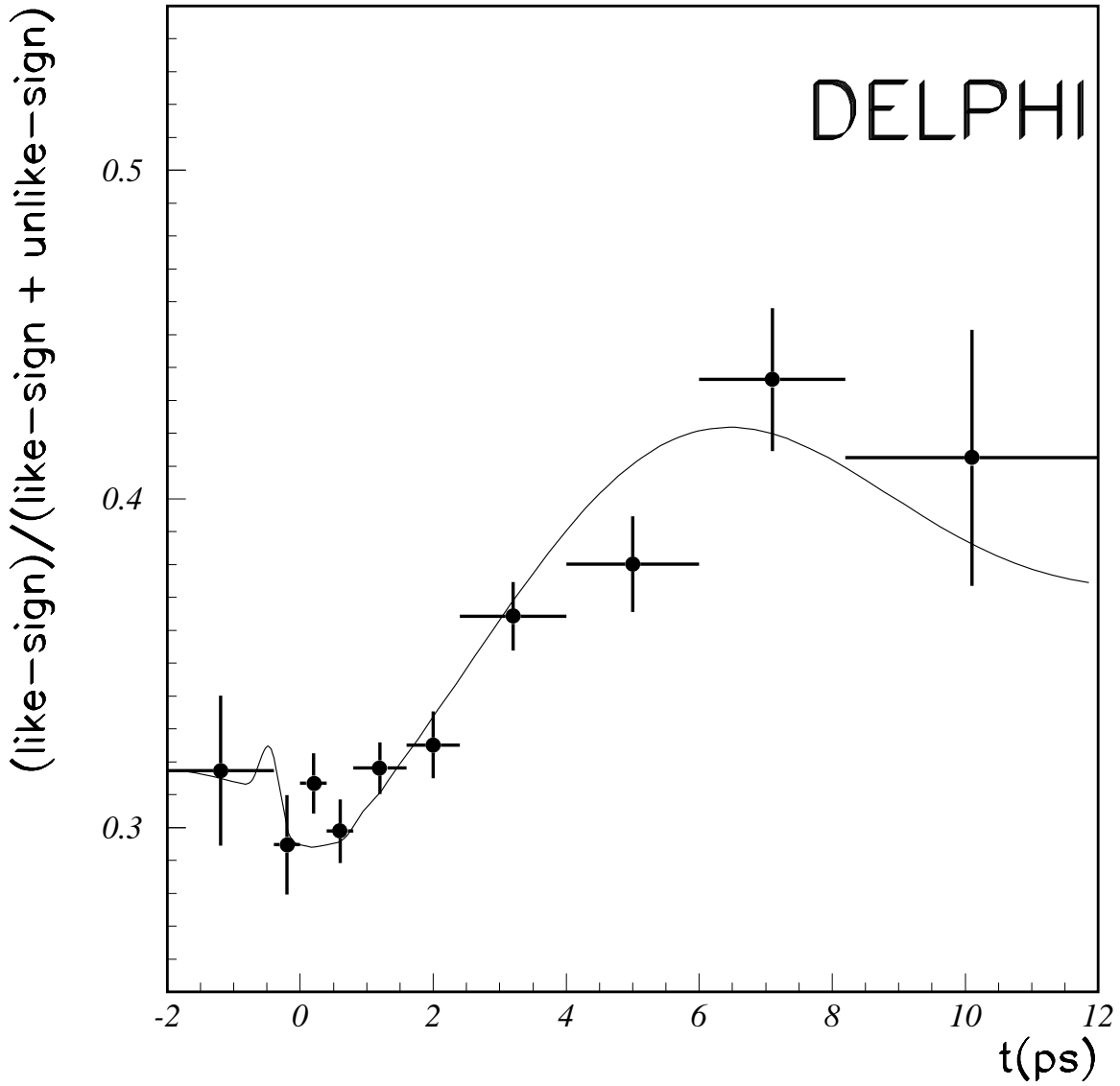


Figure 10: Fraction of mixed events versus measured time for lepton-lepton candidates. Events with two time measurements enter twice. The full line corresponds to the prediction for  $\Delta m_d = 0.480 \text{ ps}^{-1}$  projected on a single time axis.